ESA Project **METHANE+**	**FINAL REPORT**	Version: 1.0 Doc ID: TN-D15/16-CH4PLUS Date: 14-April-2023

FINAL REPORT

ESA project METHANE+ led by SRON

WP 1000, Deliverable D15/D16

Lead authors:
Michael Buchwitz, Oliver Schneising, Steffen Vanselow (Univ. Bremen), Sander Houweling, Jacob van Peet (VU), Richard Siddans, Brian Kerridge, Lucy Ventress, Diane Knappett (RAL), Cyril Crevoisier, Nicolas Meilhac (LMD), Tobias Borsdorf, Alba Lorente, Ilse Aben (SRON)

Change log

Version	Date	Status	Authors	Reason for change
0.4	15-July-2022	Draft	see title page	New document, sections 3.3.2 and 3.3.3 missing, executive summary not complete
0.9	6-April-2023	Full version	see title page	Complete report
1.0	14-April-2023	Final Version	See title page	Approved by ESA, no changes to v0.9

Executive Summary

Reducing methane emissions is top priority on the political agenda as evidenced by the Methane Pledge and initiatives like the United Nations International Methane Emission Observatory. Satellites can play a key role in providing the much-required observational data to support those climate mitigation strategies. As such, projects like Methane+ to further improve the CH_4 satellite data products and its use, are essential in this process.

The Methane+ project evolved around two main tasks. The first task was the further development of the CH_4 satellite products from the TROPOMI SWIR and the IASI Metop-B TIR instruments, in each case through the intercomparison and validation of the state-of-the-art products developed by two different groups. In addition, a combined SWIR+TIR data product was developed by combining the individual L2-data products. For each of the products a 3-year dataset was provided. The second main task in Methane+ was to use these data products to study the complementarity of the SWIR and TIR data products in estimating sources and the main sink of methane, where again two different inversion systems were used and results compared in the project. In addition, a Scientific Roadmap was developed with recommendations for future work.

For the TROPOMI CH_4 SWIR data products the intercomparisons of the two different products (WFMD Bremen, RemoTeC SRON) and the continued validation of the data, helped to identify clear aspects of the retrieval algorithms that could be further improved. In particular, systematic inaccuracies related to surface albedo features were identified and significantly reduced in the latest versions of the scientific data products. Moreover, these improvements were integrated into the TROPOMI operational processor in the processor upgrade at end of July 2022 and in the subsequent full mission reprocessing thanks to the timely delivery of the team.

The two IASI Metop-B CH_4 products (LMD, RAL) are based on distinctly different retrieval approaches which, amongst other aspects, provide different vertical sensitivities. As such, they could not be compared directly. Comparisons of the two retrieval products were performed with respect to common independent profile datasets (AirCore, ATom-4 and the CAMS GHG flux inversion v19r1). The RAL IASI product was also compared to TCCON column average volume mixing ratios in preparation for the joint use of the TIR and SWIR data. On the basis of this exercise, significant improvements were made to the RAL IASI products, in particular to reduce negative bias found at low latitudes. Further work was identified to be needed to reduce positive bias at high latitudes evident in comparisons of RAL IASI data with some correlative data sets. Disagreements between LMD and correlative data were also shown to be larger at high latitudes.
A scheme was then developed and applied for the first time to combine L2 data from TROPOMI S5P and Metop-B IASI to produce a 3-year global SWIR-TIR dataset

(March 2018- March 2021).
The column average from the combination closely tracks the TROPOMI input and the upper tropospheric and higher layers track the IASI input; consistent with their respective vertical sensitivities. Coherent positive anomalies are found in the lower tropospheric layer in association with several methane emission regions (Indo-Gangetic plain, Bangladesh wetlands, Amazonia, South Sudan and California Central Valley Indo-Gangetic plain). Accuracy of the SWIR-TIR output is wholly dependent on that of the TROPOMI and IASI inputs, so future application of the SWIR-TIR combination scheme will benefit from further improvements to both TROPOMI and IASI products as identified for future work.

As with the retrieval data products, two different inverse modeling systems (TM5-4DVAR VU, Jena CarboScope) were used in Methane+. The systems were prepared to allow the use of the various datasets from TROPOMI and IASI : TROPOMI Operational, RemoTeC and WFMD data, IASI LMD and RAL data, joint SWIR-TIR 0-6km RAL data, and the joint use of TROPOMI RemoTeC and IASI RAL data. TM5-4VAR was also adjusted to allow joint optimisation of sources and the OH-sink. Inversions were performed for a 2-year period (2018 – 2019) using all these datasets individually, except the combination of TROPOMI and IASI data. Additional 3-year inversions (2018-2020) were performed for selected retrieval products, including the combination of TROPOMI and IASI data (i.e. SWIR-TIR 0-6km RAL and joint use of TROPOMI RemoTeC + IASI RAL data).
All retrieval products lead to optimized fits that were consistent with the surface measurement network, except for the joint SWIR-TIR 0-6km RAL retrieval which TM5-4DVAR had difficulty fitting. The reason for this is not well understood yet, but deserves further attention as the combined use of the TROPOMI and IASI products to constrain the tropospheric methane column avoids biases introduced by inconsistencies in the representation of the stratospheric sub-column in the atmospheric models. Moreover, the CarboScope inversion did not show poorer agreement with the SWIR-TIR 0-6km retrieval product.
The 3-year inversions have been used to study the causes of the sharp increase in CH_4 background level during 2020. Inversions that optimize OH attribute the CH_4 increase either to increased emissions or to a reduced sink during 2020, depending on the dataset that is used. This indicates that sources and sinks are not well distinguished by the data. It is possible that more robust results could be found if the sink were given more degrees of freedom in the optimization, rather than a global, annual scaling factor.
Regional case studies were conducted to investigate the added value of the combined use of SWIR and TIR data in inversions. Generally, the results of the combined dataset are consistent with that of the separate datasets, mostly resembling the dataset that provides the strongest constraint (which varied between the cases). However, whether or not the use of more data leads to more realistic solutions cannot be concluded from the results that were obtained. While an initial validation using independent measurements was carried out, no clear conclusion

could be drawn. To better interpret the results, a more detailed evaluation using additional independent data is required.
Using the outcomes of Methane+, recommendations for further work have been formulated and are provided in detail in the Methane+ Scientific Roadmap. In short, Methane+ has provided clear areas for further improvement of the individual CH_4 retrieval products (e.g. TIR bias at high latitudes). Achieving these improvements will be key also to developing a robust SWIR-TIR data product, however, first results are considered promising. Methane+ also identified clear activities needed to further develop the inverse atmospheric modeling systems, e.g. finding the underlying cause(s) of bias with respect to SWIR and TIR satellite data for which corrections have to be applied and further optimisation of estimating the CH_4 sink. In addition, there are more general model developments needed to deal with all the different CH_4 datasets that we already have and will become available in the near future. This relates principally to increased spatial resolution, much larger data volumes, and different sampling strategies.

Contents

Reference Documents

[CH4+ Proposal] Methane+ proposal to ESA, SRON-PO-IT-2019-001, issue 1, 9 May 2019
[CH4+ RBD] Methane+ Requirements Baseline Document, TN-D1-CH4PLUS, v1.1, 10 June 2020
[CH4+ ATBD TIR] RAL IASI Methane Retrieval ATBD, v2.1, 21 July 2022
[CH4+ ATBD SWIR+TIR] RAL SWIR+TIR Methane Retrieval ATBD, v1.1, 21 July 2022
[CH4+ VR SWIR] Methane+ Validation Report-SWIR, TN-D3a-CH4PLUS, v2.0, 29 April 2022
[CH4+ VR TIR] Methane+ Validation Report-TIR and SWIR-TIR, TN-D3b-CH4PLUS, v2.1, 21 July 2022
[CH4+ DP] Methane+ Data Pool description/Auxiliary dataset User, TN-D4andD5-CH4PLUS v2.0, 22 July 2022
[CH4+ PUG] RAL SWIR-TIR L2 Methane Product User Guide, V1.0, 22 July 2022
[CH4+ SAR] Methane+ Scientific Assessment Report, TN-D8-CH4PLUS, v2.0, 9 March 2023
[CH4+ SR] Methane+ Scientific Roadmap, TN-D9-CH4PLUS, v3, 11 July 2022

1 Introduction

Methane (CH_4) is the second most important anthropogenic greenhouse gas after carbon dioxide (CO_2) and responsible for ~30% of current global warming due to greenhouse gases. Although the overall contribution of methane to global warming is less than that of CO_2, per molecule methane is a much stronger greenhouse gas, and it has a relatively short life/residence time of roughly a decade. As such, reductions in methane emissions have a faster impact on global warming and it has now been recognised at the highest international political level that the reduction of methane emissions is crucial to mitigate climate change in the near term, in addition to reducing CO_2 [UNEP-CCAC, 2021]. In Oct. 2020 the EU launched its Methane Strategy [EC, 2020] in support of the European Green Deal [EC, 2019], and at the COP26 in Nov. 2021, the Methane Pledge [MethanePledge] was signed by over 100 countries to reduce methane emissions at least 30% compared to 2020 levels by 2030.

Despite these efforts, methane is by far the largest contributor to the departure of the path to the 2ºC target of the Paris Agreement [Nisbet et al., 2020]. The average growth rate of atmospheric methane over the past 5 years is the highest since its atmospheric measurements started in the mid-1980s, with record high growth in 2020 [NOAA, 2022] despite the pandemic, and 2021 is on track of setting an even higher new record. The growth of methane in the atmosphere has shown quite some unexpected changes in the past decades. In the 90s the growth rate slowed, hovering near zero between 2000 and 2005, after which concentrations started to rapidly increase again, cumulating in the record growth in 2020. The exact causes for these changes are still scientifically debated [e.g. Worden et al, 2017; Lan et al., 2019; Lunt et al., 2019; Scarpelli et al, 2022; Zhang et al, 2021]. Moreover, these variations were not captured in any of the IPCC future scenario projections [IPCC, 2013], showing that we are not yet capable of predicting the behavior of atmospheric methane and therefore its future effect on climate change.

In order to effectively reduce methane emissions at the global scale, we thus first need to improve our understanding of the main drivers of the observed global increase of methane through a more accurate quantification of its global sources and sinks. In addition to bottom-up emission inventories, atmospheric measurements of methane are essential to improving estimates of sources and sinks. In addition to sub-orbital atmospheric measurements, satellite observations are key to providing this information on the global scale and enabling to separation of various source (and sink) contributions. However, the accuracy requirements for such methane satellite measurements are very challenging, thus putting high demands on the quality of the methane satellite products.

In Methane+ we aim to take advantage of important recent developments in methane satellite observations.
This includes the new SWIR observations from TROPOMI (launched in 2017,

operational methane product available since 2019), and the development of combining SWIR and TIR methane observations to increase the methane sensitivity/coverage over oceans and high latitudes, and to increase the methane vertical height information from satellite observations to better separate the sources and the main chemical sink via the hydroxyl radical (OH).

Another new opportunity - in support of reducing methane emissions - is provided by the improved spatial resolution and coverage of satellite methane observations from TROPOMI. This capability enables the detection and identification of methane super emitters (e.g. huge point sources emitters). TROPOMI for the 1st time provides information on these super emitters on a global scale, even using only single overpasses (e.g. Pandey et al., 2019; Lavaux et al, 2021; Schuit et al., 2023).

In order to support further exploitation of methane satellite measurements for the purpose of more accurate quantification of methane sources and sinks, the Methane+ project focused on the following specific original study objectives [CH4+ Proposal, 2019] :

- Support the algorithm development for the SWIR retrieval from TROPOMI and joint SWIR-TIR retrieval from TROPOMI and IASI/CrIS.
- Assess the quality of the TROPOMI, IASI and CrIS XCH_4 retrieval: comparing algorithms and validation using independent ground-based data.
- Investigate the added value of combining SWIR and TIR in regional case studies
- Infer global sources and sinks of CH_4 from inverse modelling of 2 years of TROPOMI and IASI (and/or CrIS) data, investigating the added value of the combined use of SWIR and TIR
- Investigate the consistency of the SWIR and TIR retrieval datasets, with model simulated transport and chemistry.
- Formulate a road map for future CH_4 remote sensing based on the outcomes of this study as well as parallel studies covering the use of methane from TROPOMI across the full range of scales.

In this project we combine a team of world-leading experts on SWIR TROPOMI XCH_4 retrievals (SRON, and IUP-Bremen), TIR IASI CH_4 retrievals (RAL and LMD), as well as inverse atmospheric modeling experts (VU and MPI-BGC/DLR). For each of these three key domains we have two different partners in the consortium to ensure that independent approaches/algorithms are applied to the same problem. This allows for intercomparisons, with the aim to improve individual products/approaches and get a better sense of uncertainties. A more detailed description of the track records of the partners in Methane+ can be found in the Methane+ proposal [CH4+ Proposal, 2019].
The project evolves mainly around the two main WPs. WP2000 is the WP which deals with all the retrieval activities (retrieval developments incl. combined TIR+SWIR data product, validation, intercomparisons, generation of minimal two-year datasets),

and WP3000 is the WP with all the atmospheric modeling and flux inversion activities (incl. pre-processing of the data for ingestion into the model, model-specific bias correction, development of OH optimisation, evaluation against independent measurements, science case studies). More details about the various datasets, retrieval algorithms, validation datasets, transport models and inverse modeling approaches, target comparison regions, foreseen science cases, etc. can be found in the Requirement Baseline Document [CH4+ RBD, 2020].

The deliverables of the Methane+ project consists of the various satellite datasets[1] for -at least- the period Jan. 2018 – end 2020, as well as various documents as listed in Table 1. These can all be accessed through (links on) the project website: www.methaneplus.eu

This Final Report aims at providing an overview of the project, focussing on the main developments and outcomes, without duplicating all detailed descriptions and results which can be found in the various document deliverables referenced here.

The Methane+ project kicked off on 20th Jan 2020 and had its Final Review on 24 June 2022. The team was never able to meet in person due to COVID restrictions, so all Progress Meetings (incl. KO and FR) were done remotely.

Table 1: All Methane+ deliverables.

[1] Some (parts) of datasets were developed and generated through other projects such as C3S, CCI+ and NSO TROPOMI. Methane+ guaranteed early data access for the partners in the project.

#	Item Identifier	Title	Versions, date	Reference
D1	RB	Requirements Baseline Document	V1.1, 10 June '20	[CH4+ RBD]
D2	ATBD	Algorithm Theoretical Baseline Document	VI, TIR, 9 April 2021 V2.1, TIR, 21 July 2022 V1.1 TIR+SWIR,21 July'22	[CH4+ ATBD TIR] [CH4+ ATBD SWIR+TIR]
D3	VR	Product Validation Report	V2, SWIR, 29 April '22 V1, TIR, 14 May 2021 V2.1, TIR, TIR+SWIR, 21 July 2022	[CH4+ VR SWIR] [CH4+ VR TIR]
D4/D5	DP	Data Pool to be published & Auxilliary dataset User Manual	V0.9, 3 June'20 V2, 22 July 2022	[CH4+ DP]
D6	OP	Output Products		https://ftp.sron.nl/open-access-data-2/TROPOMI/tropomi/ch4/18_17/ https://www.iup.uni-bremen.de/carbon_ghg/products/tropomi_wfmd/ https://catalogue.ceda.ac.uk/uuid/4bbcb1722f2842c1b0a5ebc19160a863 https://iasi.aeris-data.fr/ch4/
D7	PUG	Product User Guide	V1, TIR+SWIR, 22 July '22	[CH4+ PUG]
D8	SAR	Scientific Assessment Report	V2.0, 9 March '23	[CH4+ SAR]
D9	SR	Scientific Roadmap	V3, 11 July 2022	[CH4+ SR]
D10	WEB	Project website		methaneplus.eu
D15/16/11/12/13	FR/ ES/PRO/MM	Final Report & Executive Summary & Promotion, multimedia summary report & scientific pub.	V1, 14 April 2023	This report

2. CH_4 data products (WP2000)

2.1. Introduction

The aim of WP2000 was to provide improved methane data products that have been used for inverse modelling in the second phase of the project. The observations that have been used to create the methane data products include measurements from the short-wave infrared (SWIR) spectral band from the TROPOMI instrument onboard the Sentinel-5P satellite, and measurements from the thermal infrared (TIR) spectral band from the IASI instrument onboard the Metop B satellite. Retrievals from the SWIR provide good vertical sensitivity to the total column-averaged dry-air mole fraction of methane (XCH_4). Retrievals from the TIR can additionally provide vertical information of the trace gas distribution that can be of great interest for inverse modelling.

SRON developed an improved TROPOMI XCH_4 retrieval algorithm that is based on the full-physics approach. The SRON S5P-RemoTeC XCH_4 provides an enhanced global coverage with respect to previous versions by including retrievals under sun-glint geometries over water bodies and deploying a more advanced posterior correction. IUP-UB provides another scientific XCH_4 data product derived from the TROPOMI SWIR measurements. It is based on the Weighting Function Modified Differential Optical Absorption Spectroscopy (WFM-DOAS or WFMD) retrieval algorithm, which is a linear least-squares method based on scaling (or shifting) preselected atmospheric vertical profiles, and it applies an enhanced post-processing of the XCH_4 retrievals based on machine learning techniques. The two datasets have been validated with ground-based TCCON measurements and extensively intercompared to demonstrate their complementary value for inverse modelling [CH4+ VR SWIR].

RAL processed the IASI Metop B data to provide a global height-resolved dataset based for use in inverse modelling for the same period as S5P. Following a validation exercise, modifications were made to this TIR scheme which was then re-evaluated against correlative data. Furthermore, a scheme was implemented to combine SWIR retrievals from S5P with TIR retrievals from IASI via a post-processing scheme that accounts for the different vertical sensitives of the retrievals. Data from the combination were validated in the same way as the IASI-only data and surface-450hPa (~0-6km) layer data were evaluated in the inverse modelling systems.

The possibility to use TIR retrievals from Suomi-NPP CrIS (better co-located with S5P) was investigated, applying the IASI retrieval scheme to CrIS. However, it was found that the information content for methane was considerably reduced for CrIS compared to IASI, because of the difference in spectral resolution. Furthermore, a problem with the Suomi-NPP CrIS instrument meant there are no measurements in the methane band for a period of approximately three months in the middle of our study period (March-June 2019). The project therefore focused on TIR retrievals from IASI (and their combination with S5P).

LMD provided the reprocessed LMD IASI/Metop-B mid-troposheric columns of CH_4 (MT-CH_4) version 9.1 for 2018-2020, which correspond to the official IASI Level 2 product that are assimilated by ECMWF for CAMS reanalysis. These retrievals have been validated using AirCore profiles and using the ATom aircraft-based profiles (Wofsy et al., 2018), extrapolated with CAMS v19r1. Furthermore, the LMD IASI-B MT-CH_4 have been compared with the CAMS v19r1 model, in term of global distribution, interesting regions and time series.

2.2. SWIR TROPOMI

SRON Netherlands Institute for Space Research develops the retrieval algorithm for the operational processing of TROPOMI XCH_4 data by ESA. In the software deployment cycle, SRON provides a scientific beta product that already includes updates and improvements of the XCH_4 retrieval. SRON focused in this project on providing the SRON S5P-RemoTeC scientific TROPOMI XCH_4 product with the latest updates that were developed over the course of Methane+. The Institute of Environmental Physics of the University of Bremen (IUP-UB) provided TROPOMI XCH_4 data retrieved with the scientific algorithm WFMD.

Besides providing the data products, a major goal in the project has been to assess the data quality of the different products by validation with external, independent reference measurements and to work out differences between the data products through detailed inter-comparison [CH4+ VR SWIR].

2.2.1. SRON TROPOMI data product

SRON provided TROPOMI XCH_4 data retrieved with the latest improvements of the S5P-RemoTeC full-physics retrieval algorithm. A first version (version 14_14) included improvements related to the regularization scheme, the selection of the spectroscopic database, and an a posteriori correction for the albedo dependence, fully independent of any reference data, derived using only TROPOMI XCH_4 data [Lorente et al., 2021]. This correction is more accurate than the one implemented at the beginning of the mission, as it more strongly corrects the XCH_4 underestimation at low surface albedo. This product was further improved to include retrievals for measurements over the ocean under sun-glint geometries (version 17_18). These retrievals do not show a specific dependence on signal or albedo, as do data over land, so we apply an overall scaling factor to homogenize the XCH_4 distribution over land and ocean. All these updates have resulted in a TROPOMI XCH_4 product with high quality, as demonstrated by the validation with independent ground-based measurements from the Total Carbon Column Observing Network (TCCON) and the comparison with GOSAT satellite XCH_4 data. Furthermore, we have performed a comparison with the WFMD IUP-UB product over regions that are challenging for the retrieval, to assess the developments [CH4+ VR SWIR].

The SRON S5P-RemoTec scientific XCH_4 dataset is validated with independent XCH_4 retrievals from ground-based Fourier Transform measurements (FTIR) performed by the TCCON network. For each TCCON station we calculate a mean bias and its standard deviation from the time series of collocated XCH_4 retrievals which quantifies the data quality on a regional scale. To analyze the global agreement between TCCON and TROPOMI, we compute the average of the station biases and its standard deviation as a measure of the station-to-station variability. For version 14_14, the average bias for all the stations was -0.2% (-3.4 ppb) and the station-to-station variability was 0.3% (5.6 ppb). Before the correction, the agreement was -0.9% (-17 ppb) and the station-to-station variability was 0.6%. For version 18_17 the average bias for all the stations is -0.3% (-5.4 ppb) and the station-to-station variability is 0.3% (5.1 ppb). From this we can conclude that the scientific SRON S5P RemoTeC TROPOMI XCH_4 data set is well within the mission requirements for accuracy and precision (below 1%), even before the posterior correction is applied.

For the comparison with satellite data, we use the GOSAT proxy XCH_4 data product retrieved with the RemoTeC/proxy retrieval algorithm. For the analysis over land, we compare XCH_4 retrieved from TROPOMI (version v14_14) and GOSAT measurements for a period of 2 years (January 2018-December 2019). The comparison yields a mean bias of -10.3 ± 16.8 ppb. We perform a similar comparison for version 18_17, including ocean measurements over sun-glint geometries for the period 1 March 2018–31 December 2020. Over land, the comparison results in a bias after correction of -13.8 ± 16.1 ppb (-0.7 ± 0.8 %). Over ocean, the comparison results in a bias of -4.4 ± 15.7 ppb (-0.2 ± 0.9 %).

Regions from around the world were identified that are challenging from the point of view of XCH_4 retrievals, covering scenes with occasional snow cover (high latitudes), with albedo-aerosol interactions (Australia), for high (North Africa) and low surface albedos (Canada, Russia) as well as over the ocean. For the inter-comparison of the SRON (version 14_14) and WFMD data products, we calculated global monthly averaged maps over these regions at a a spatial resolution of 0.1° x 0.1°. An example of the monthly averaged data used for the comparison is show in Figure 1 for Australia and North Africa. The complete analysis is documented in the Validation Report [CH4+ VR SWIR].

In general, the comparison of the products shows that the SRON TROPOMI XCH_4 dataset is biased low with respect to the WFMD IUP-UB. The posterior bias correction reduces the dependencies with surface albedo. This is the case over Australia, for example, where before the correction each of the XCH_4 products has a positive correlation with the retrieved surface albedo, which becomes lower after correction. Over high surface albedo scenes (e.g., Sahara) both WFMD and SRON XCH_4 show a correlation with surface albedo before the correction is applied, with higher XCH_4 retrieved for high surface albedo scenes. This effect is corrected for by the posterior correction that is applied in both products.

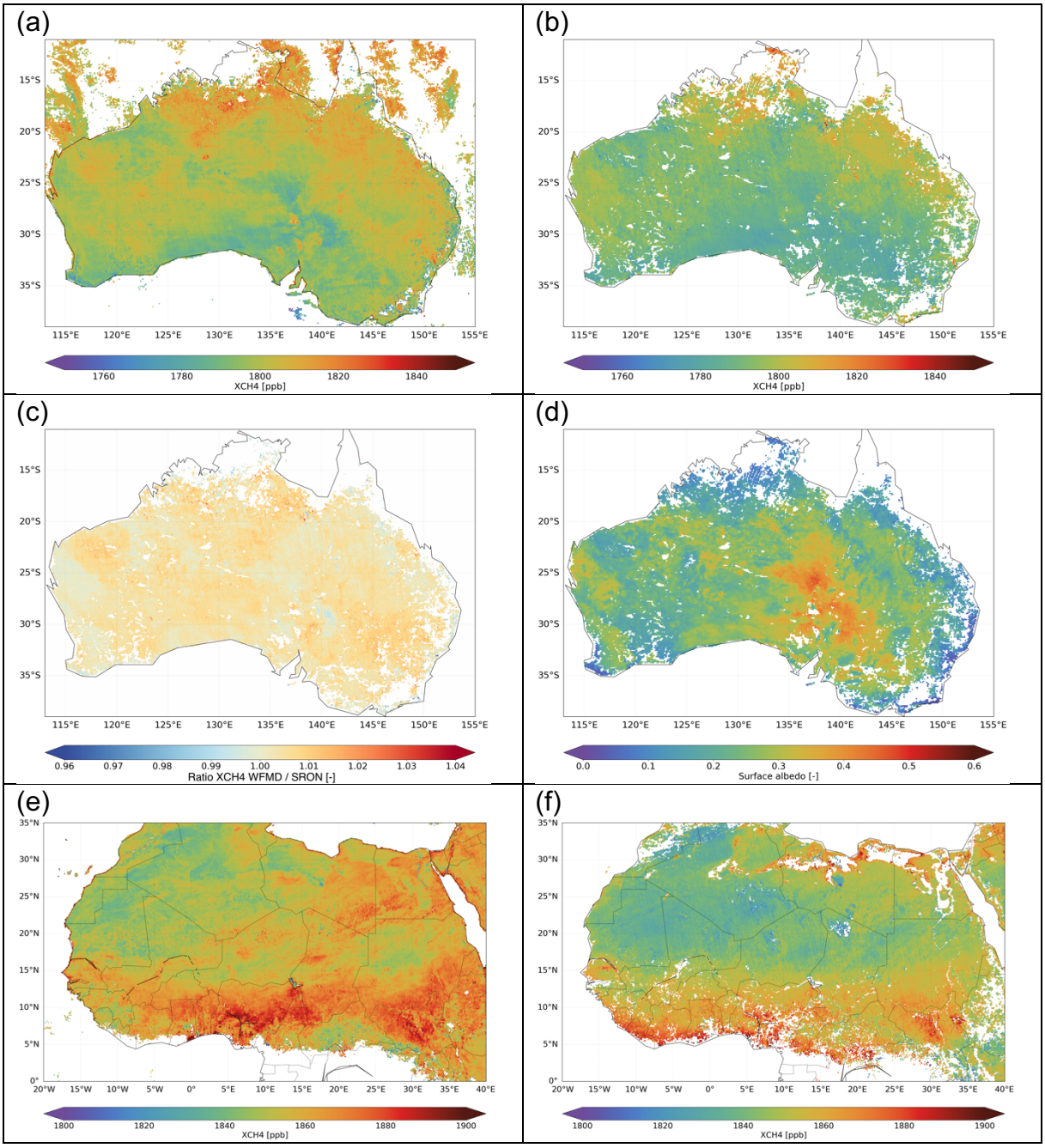
(a)
(b)
(c)
(d)
(e)
(f)
XCH4 [ppb]
Ratio XCH4 WFMD / SRON [-]
Surface albedo [-]

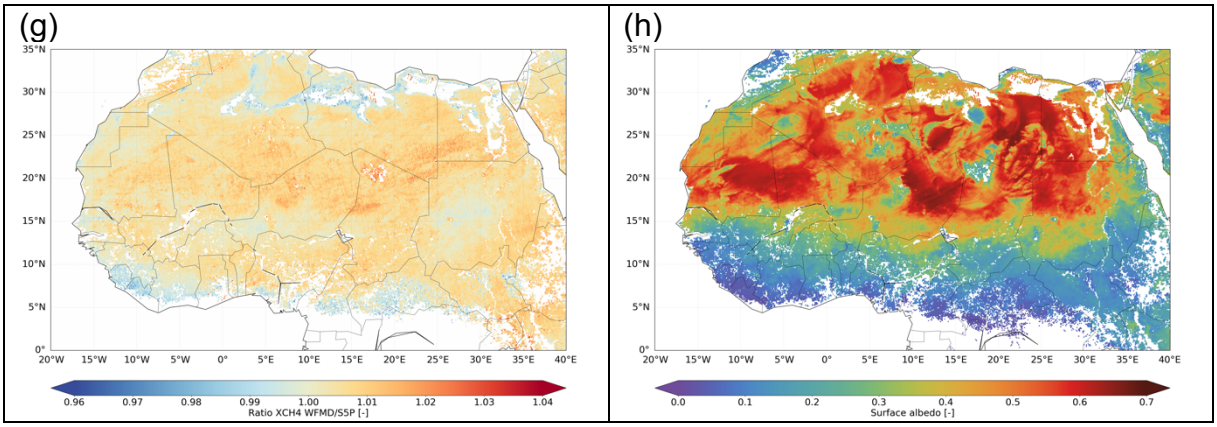

Figure 1 TROPOMI XCH_4 retrieved by (a, e) IUP-UB with WFMD (b, f) SRON with the scientific S5P RemoTeC algorithm, WFMD/SRON XCH_4 ratio (c, g) and (d,h) SWIR surface albedo retrieved by SRON.

Figure 2 shows the monthly mean XCH_4 for each product with its standard deviation for Australia (a) and North Africa (b). Both products follow a similar seasonality in the distribution of XCH_4 so both capture correctly the geophysical variation of XCH_4. The bias is negative (WFMD XCH_4 higher than SRON XCH_4) for the complete time period, and for the case of Australia, it shows a slight increase with time (Figure 2a). Over North Africa (Figure 2b), January and February 2019 are the months when the bias between the two products is higher for this specific region, where SRON retrieves a stronger decrease in XCH_4 than WFMD does.

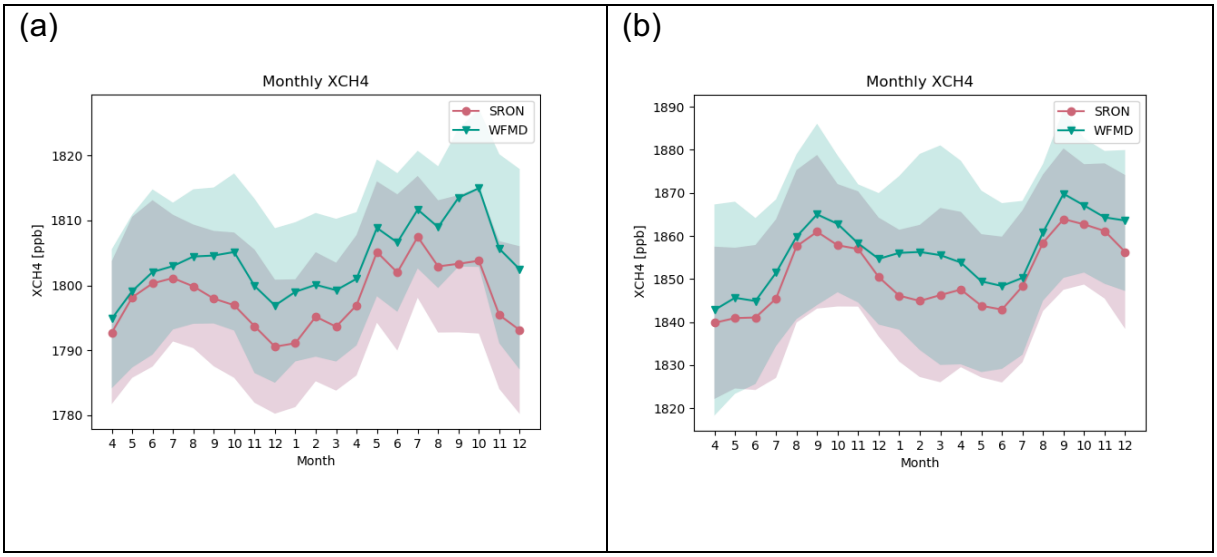

Figure 2 Monthly mean XCH_4 retrieved by SRON (red) and WFMD (green) with the 1-sigma standard deviation represented by the shadowed areas for (a) Australia and (b) North Africa from April 2018 through December 2019.

In the last phase of the project, research was conducted into the way the spectral dependence of the surface reflectance is handled in the inversion [CH4+ VR SWIR].

In version 14_14 and 18_17, the fit includes a 2nd order polynomial. It has been shown that increasing the order to 3 improves the representation of surface features in the retrieval. This modification of the spectral fit removes artifacts (discovered with the SRON and WFMD comparison) related to the underlying surface features, significantly improving the XCH_4 data product. This is the case over Northern Siberia, in Russia. Figure 3 shows that the significant XCH_4 enhancement in version 18_17 (Figure 3a) is removed when increasing the order of the polynomial (Figure 3b) and that the fit quality significantly improves. Over the Sahara Desert, several XCH_4 enhancements related to specific surface features (e.g., over Algeria) are also removed when increasing the order of the polynomial. In other areas, this modification results in higher XCH_4 (although with smaller effect), which is also an improvement as these are typically areas with low albedo where the SRON S5P-RemoTeC XCH_4 product underestimates XCH_4. The improved S5P-RemoTeC full-physics retrieval incl. the 3rd order polynomial fit will already be implemented in the next version of the operational processor (v2.4.0) expected to be activated by August 2022.

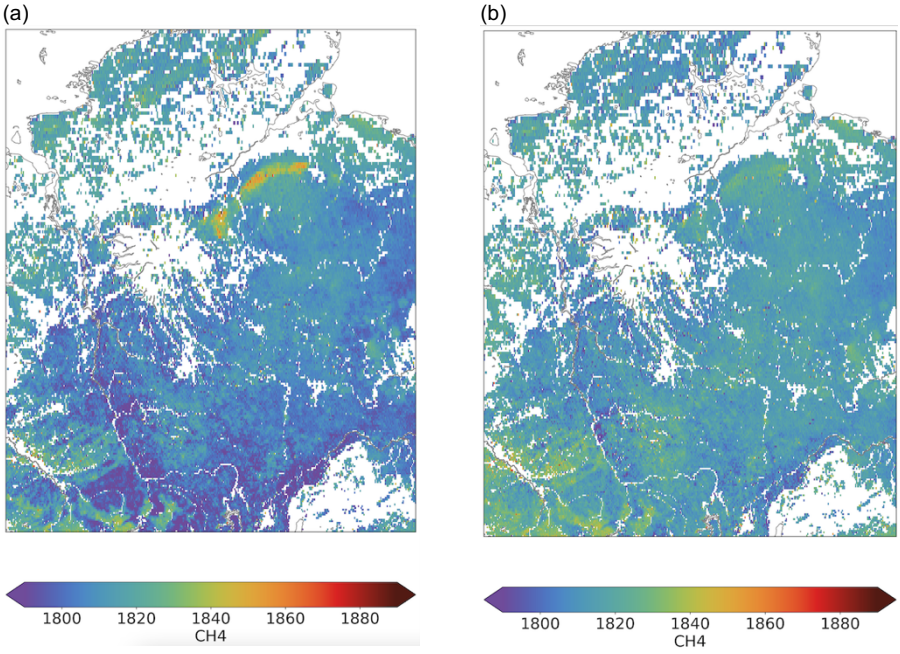

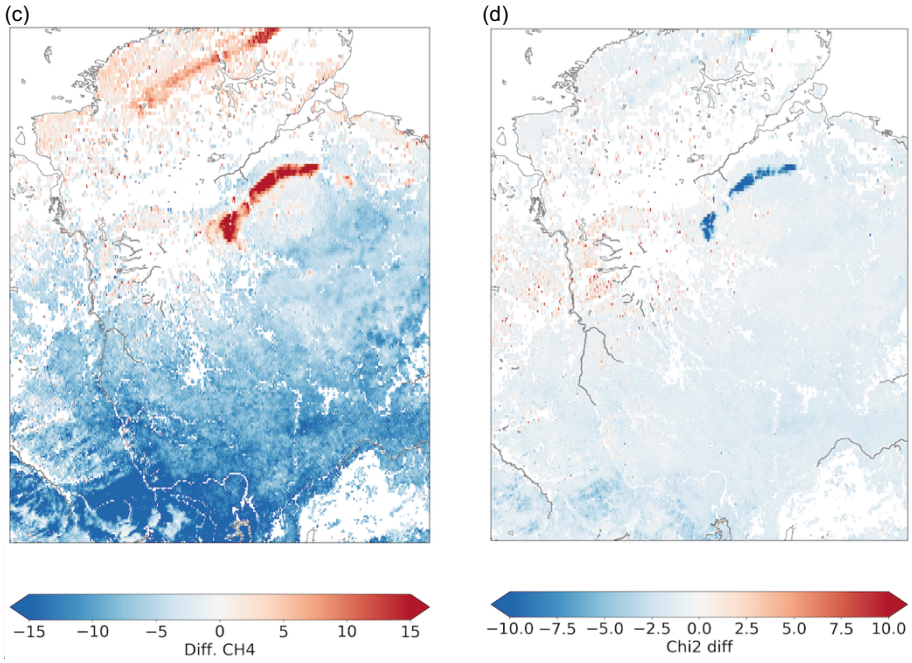

Figure 3 XCH_4 averaged on a 0.1° x 0.1° grid retrieved with (a) a second-order polynomial and (b) a third-order polynomial for the fit of the surface reflectance spectral dependence. (c) Difference between (a) and (b) and, (d) the difference in χ^2 for each of the retrievals.

2.2.2. IUP TROPOMI data product

The Institute of Environmental Physics of the University of Bremen (IUP-UB) provided TROPOMI XCH_4 data retrieved with the scientific algorithm "Weighting Function Modified Differential Optical Absorption Spectroscopy" (WFM-DOAS or WFMD) [Schneising et al., 2019]. The related analyses performed in this project were focused on the validation of the WFMD XCH_4 data as well as the comparison with the operational Copernicus TROPOMI XCH_4 product (V01.02.02) and the scientific SRON TROPOMI XCH_4 product (v14_14) [Lorente et al., 2021] for selected regions exhibiting locally elevated methane. The baseline WFMD XCH_4 version within this project was v1.2, but additional comparisons were also carried out using the further improved WFMD data version 1.5. All TROPOMI WFMD data sets include measurements over the ocean and inland water and have significant coverage at high latitudes. Intense methane sources are readily detected in a single satellite overpass, e.g., methane leakage from natural gas production [Schneising et al., 2020].

The WFMD data are validated using the GGG2014 collection of the Total Carbon Column Observing Network (TCCON), providing realistic error estimates of the satellite data. To ensure comparability, all TCCON sites use similar instrumentation and a common retrieval algorithm. The TCCON data are tied to the WMO trace gas scale using airborne in situ measurements, applying individual scaling factors for each species. The estimated TCCON accuracy (1σ) is about 3.5 ppb for XCH_4.

The results for the individual TCCON sites are condensed to specific figures of merit for the overall quality assessment of the satellite data. For the baseline version v1.2, the global offset relative to TCCON amounts to 0.7 ppb, the random error is 14.1 ppb, and the systematic error is given by 4.5 ppb. For the upgraded product v1.5, with improved input databases (surface and meteorological information) and improved post-processing regarding quality filtering and bias correction, we get better coverage and less outliers, resulting in more collocations with TCCON and a reduced random error of 12.9 ppb at the same time. For both versions, the validation with this independent reference demonstrates that XCH_4 is retrieved well within the mission requirements after quality filtering.

The comparisons of the WFMD product (v1.2) with the SRON operational and scientific products were performed for several target regions with locally elevated methane, including anthropogenic source regions such as Turkmenistan (gas and oil production) or the Central Valley in California (oil production and agriculture) as well as natural sources such as wetlands, for example in Sudan. The comparisons of the WFMD and operational product typically show quite consistent results with reasonable to good agreement for daily spatially-resolved XCH_4 data. The correlation coefficient is typically in the range 0.5 to 0.9 depending on area and time period, but the differences of the maps also show complex patterns of large-scale and small-scale features, which are currently not well understood. The WFMD product typically has much better coverage (depending on day and region, the WFMD product has typically 2-7 times more retrievals that pass the quality screening compared to the operational product). Comparisons with the scientific SRON product show a slightly better agreement with WFMD than the operational product with respect to the number of observations and the linear correlation of the spatial patterns. Moreover, the standard deviation of the differences is somewhat reduced. Despite the slightly better agreement with WFMD, there are no substantial changes between the operational and scientific SRON products for the analysed regions and there are still significant differences compared to the WFMD product. Figure 4 shows an example of such a comparison for selected regions and days; the complete analysis is documented in the Validation Report [CH4+ VR SWIR].

Furthermore, additional comparisons with the latest version of the WFMD product (v1.5) were performed for several regions. Based on these comparisons it is concluded that the WFMD v1.5 product is improved compared to v1.2 in terms of accuracy and coverage. Nevertheless, there are also some areas of potential biases, such as over the Etosha Pan in Namibia. Although the increment over this wetland region is smaller compared to v1.2, it is probably still overestimated in v1.5. It was demonstrated with an experimental setup (to be included in the next product version) that this methane enhancement can be significantly reduced to a more realistic level (without changing other spatial patterns) by increasing the degree of the polynomial in the fit from 2 to 3, indicating an issue with spectral albedo variation in the fitting window for this singular region.

Based on these comparisons it is also concluded that the operational product (V01.02.02) shows high bias patterns in parts of Northern Siberia related to surface spectral features that are not properly accounted for in the operational algorithm (see Figure 5). These bias patterns have been misinterpreted in the literature as actual methane release from carbonate rock formations [Froitzheim et al., 2021].

In summary, the analyses performed in this project underlined the importance of better accounting for the spectral variability of albedo within the fitting window (besides the mean albedo in the continuum). This was already recognised in the generation of the current WFMD product (v1.5), which exhibits improved accuracy compared to v1.2 due to an improved bias correction that at least partially takes spectral albedo variations in the fitting window into account. The importance of spectral albedo was further corroborated by the finding that singular questionable enhancements still present in v1.5 become more realistic in magnitude after adjustment of the polynomial degree of the fit. As this finding will be accounted for in the WFMD algorithm, the project has contributed to a better quality of future versions of the methane data product.

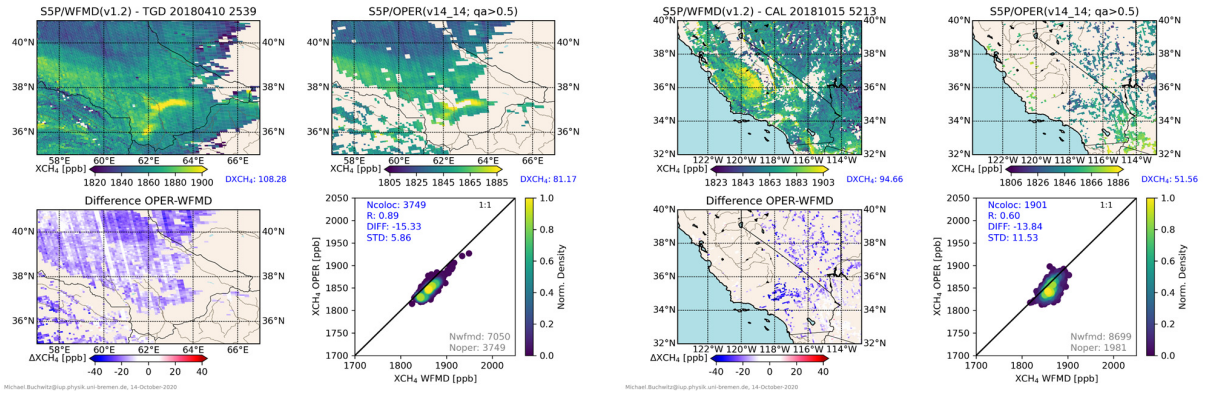

Figure 4: Comparisons of daily WFMD XCH_4 with the scientific SRON product (version 14_14) from Lorente et al., 2021 for source regions in Turkmenistan and California.

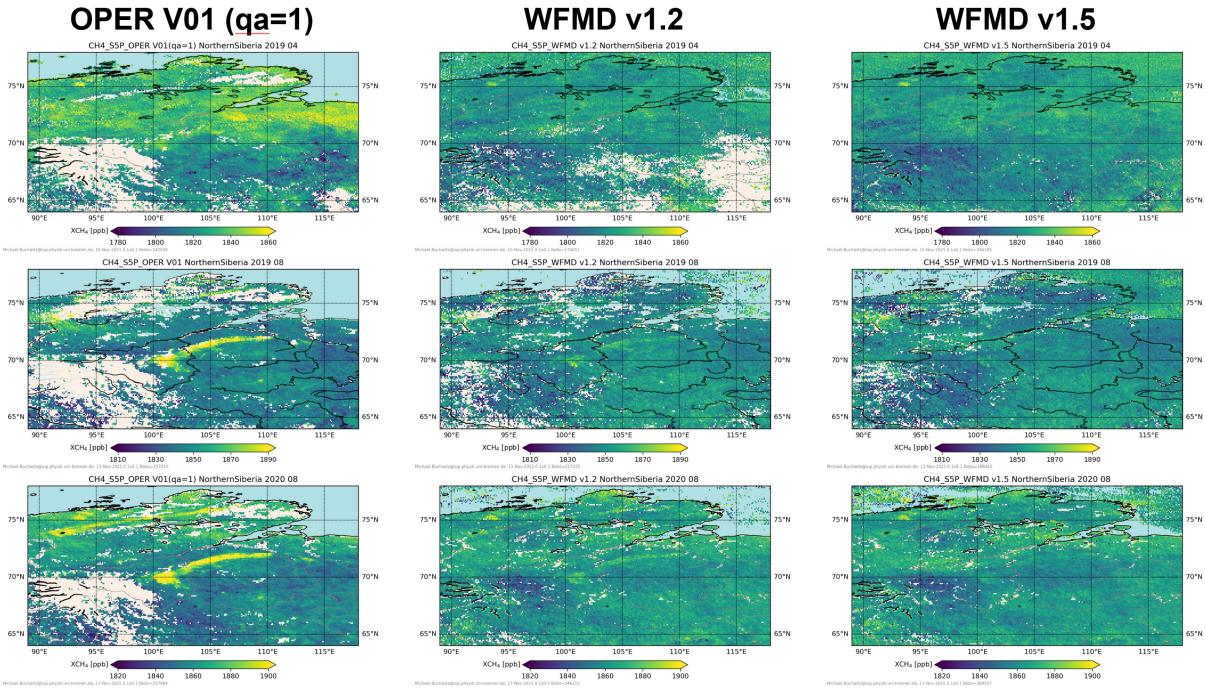

Figure 5: Comparison of three TROPOMI XCH4 data products over Northern Siberia. Top row: April 2019, middle row: August 2019, bottom row: August 2020. The bias pattern is clearly visible in the operational product (left column), hardly visible in the WFMDv1.2 product (middle column) and essentially not present in the WFMDv1.5 product with improved post-processing (right column).

2.2.3. Summary

Regarding the TROPOMI SWIR XCH_4 products, the focus in the project has been on one hand to provide two scientific XCH_4 datasets (SRON S5P-RemoTeC scientific and WFMD) for -at least- the period Jan 2018-Aug 2020 as input to the inverse modellers, and on the other hand to validate and compare these scientific products to assess their quality. SRON focused on the comparison with WFMD product over regions that are challenging for the retrieval to asses that the developments implemented in the SRON S5P-RemoTeC scientific product were correcting in the right direction. IUP-UB focused on the comparison of selected regions showing locally elevated methane, which is important in order to reliably obtain methane emission information from these data sets.

The validation with independent ground-based measurements from the TCCON network show that both scientific retrieval algorithms provide a XCH_4 product that is within the mission requirements of 1%. The inter-comparison between the two products over challenging regions shows that the SRON TROPOMI XCH_4 dataset is biased low with respect to the WFMD IUP-UB. The posterior bias correction reduces the dependencies with surface albedo.

For the regions with highly elevated XCH_4, comparisons with the scientific SRON product show a slightly better agreement with WFMD than the operational product with respect to the number of observations and the linear correlation of the spatial patterns.

The information provided by the validation and intercomparison was crucial for the next steps of the project in which these data products have been assimilated in the inverse modelling systems to infer fluxes global fluxes. Furthermore, the analyses performed in this project helped to identify particular aspects of the retrieval algorithms that led to improvements of both scientific data products beyond the versions delivered within the project timeframe, contributing to a better quality of upcoming versions of the WFMD and S5P-RemoTeC XCH_4 products. The improvements to the latter algorithm will flow directly into the official TROPOMI Sentinel-5P ESA XCH_4 operational product.

2.3. TIR IASI

This study considered data from two retrieval schemes which have been developed for the Infrared Atmospheric Sounding Interferometer (IASI) on the MetOp series of satellites. The RAL scheme (Siddans, 2017, 2020) uses optimal estimation to retrieve height-resolved information provided as column average, surface-450hPa (~0-6km) and 450-175hPa (~6-12km) layer-average mixing ratios. The LMD scheme (Crevoisier, 2009a, 2009b, 2013) uses a neural network approach to retrieve a mid-tropospheric layer average mixing ratio. Validation work focused exclusively on data from Metop-B IASI measurements in 2018 and 2019. Data were subsequently processed through to March 2021. In this period, MetOp-B was the principal MetOp satellite[2] and TROPOMI on Sentinel-5 Precursor was observing methane concurrently in the SWIR.

Because the RAL and LMD schemes have different vertical sensitivities, it is not possible to compare them directly. Independent comparisons of the two schemes were performed with respect to common independent profile datasets (AirCore, ATom-4 and the CAMS GHG flux inversion v19r1). RAL results for column average were also compared with TCCON and with Sentinel-5P in preparation for joint use of TIR and SWIR data (Section 2.4).

2.3.1. RAL IASI-B data product

The RAL scheme uses optimal estimation to retrieve height-resolved methane information from IASI soundings in the 7.9 μm (ν_4) band and co-retrieves a number of geophysical variables. The scheme takes as input atmospheric temperature and humidity profiles, surface temperature and spectral emissivity pre-retrieved from IASI and co-located MHS and AMSU-A soundings by RAL's Infrared and Microwave Sounder (IMS) core scheme (Siddans et al., 2018).

[2] MetOp-A was continuing to observe from a drifting orbit and MetOp-C was newly launched.

A key aspect of the scheme is that it exploits nitrous oxide (N_2O) absorption in the same spectral band to account for the effects of residual cloud on the retrieved methane. RTTOV (Saunders et al., 2018) is used as the radiative transfer model.

Data produced by two versions of the RAL scheme were validated within this study. The first data set (Methane+ Version 1) was used in inverse modelling tests (Section 3), the second (Methane+ Version 2) was produced by a scheme which had been modified based on findings from validation of Version 1 with the aim of improving accuracy. Only a subset of data (sufficient for the validation exercise) was processed with the modified V2 scheme. Global maps of seasonal averages are compared to CAMS in Figure 6.

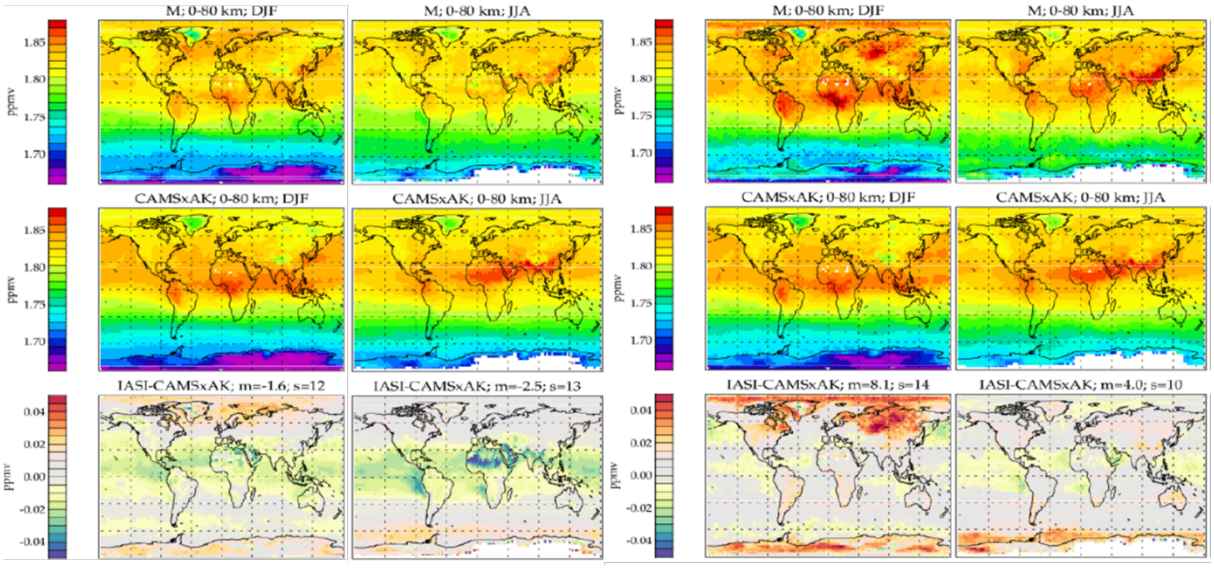

Figure 6: Comparison of seasonal average IASI (RAL Methane+ V1 and V2) column average methane mixing ratio (top row) with CAMS (flux inversion v19r1), with averaging kernels applied (middle row), and the difference between them (bottom row). Columns show (from left to right): V1 data for December-January-February (DJF, 2018 and 2019 combined); V1 data for June-July-August (JJA, 2018 and 2019 combined); V2 data for DJF; V2 data for JJA. The title above the bottom panel gives the mean ("m") and standard deviation ("s") of the differences in units of ppb.

In general, the quality of the V1 IASI-B data retrieved by the current RAL scheme was found to be comparable to that found previously for IASI-A using the same retrieval scheme. Comparisons over the two years analysed with the CAMS GHG flux inversion v19r1 showed agreement generally within +/- 20 ppbv (after accounting for retrieval vertical sensitivity by applying the averaging kernels), with V1 IASI-B lower by up to 20 ppbv in tropical latitudes and higher by up to 20 ppbv at high latitudes. The bias was also found to be somewhat dependent on the scan angle, with the largest negative biases occurring at the edge of the swath in the tropics (see

Figure 7).

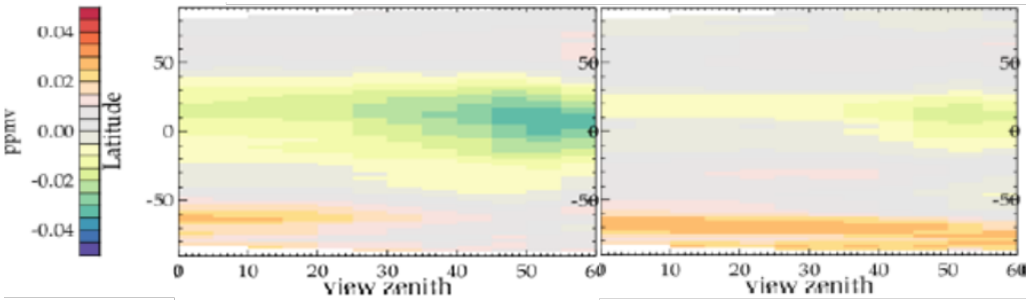

Figure 7: Difference between summer mean IASI (RAL Methane+ V1 and V2) column average methane mixing ratio and CAMS (flux inversion v19r1), with averaging kernels applied, as a function of latitude (y-axis) and viewing zenith angle (x-axis). Left-hand panel shows V1 data; right-hand panel shows V2 data.

Exceptions to this general behaviour included areas of the Sahara, the Arabian Peninsula, Greenland and Antarctica where IASI-B differences from CAMS show more spatial structure. Some are due to retrieval problems associated with spectrally-dependent surface emissivity (over desert) and low sensitivity (over cold surfaces). A specific anomaly over the southern Venezuelan highlands was caused by an error in the surface elevation model (and subsequently eliminated in the V2 data). Comparisons to independent satellite, ground-based and airborne data (S5P, TCCON, ATom-4 and AirCore) largely confirmed the general latitude-dependent bias found in comparisons to the CAMS flux inversions. This is illustrated here in Hovmöller plots comparing IASI with CAMS (Figure 8) and TCCON (Figure 9). Figure 10 shows the comparisons with TCCON in the form of a scatter plot.

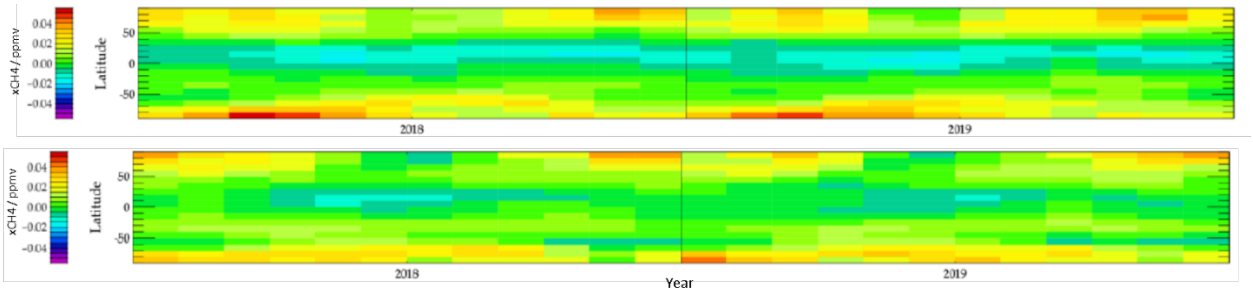

Figure 8: Hovmöller plots (month vs latitude) showing the difference between IASI (RAL Methane+ V1 and V2) column average methane mixing ratio and CAMS (flux inversion v19r1), with averaging kernels applied. Top panel shows V1 data; bottom panel shows V2 data.

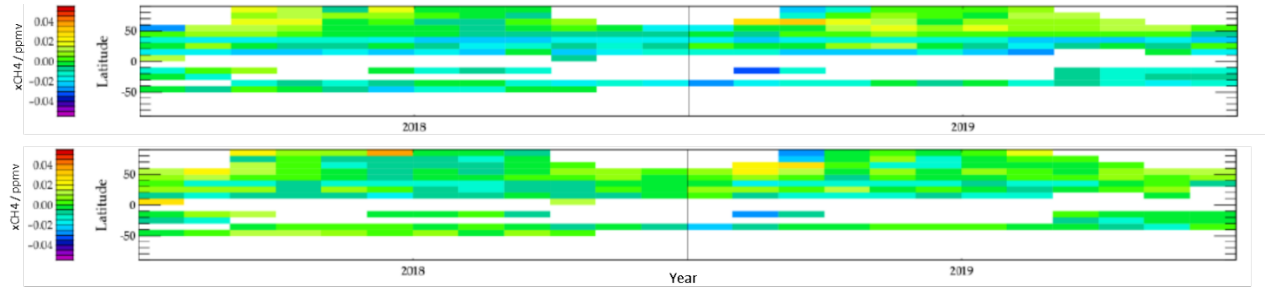

Figure 9: Hovmöller plots (month vs latitude) showing the difference between IASI (RAL Methane+ V1 and V2) column average methane mixing ratio and TCCON. Top panel shows V1 data; bottom panel shows V2 data.

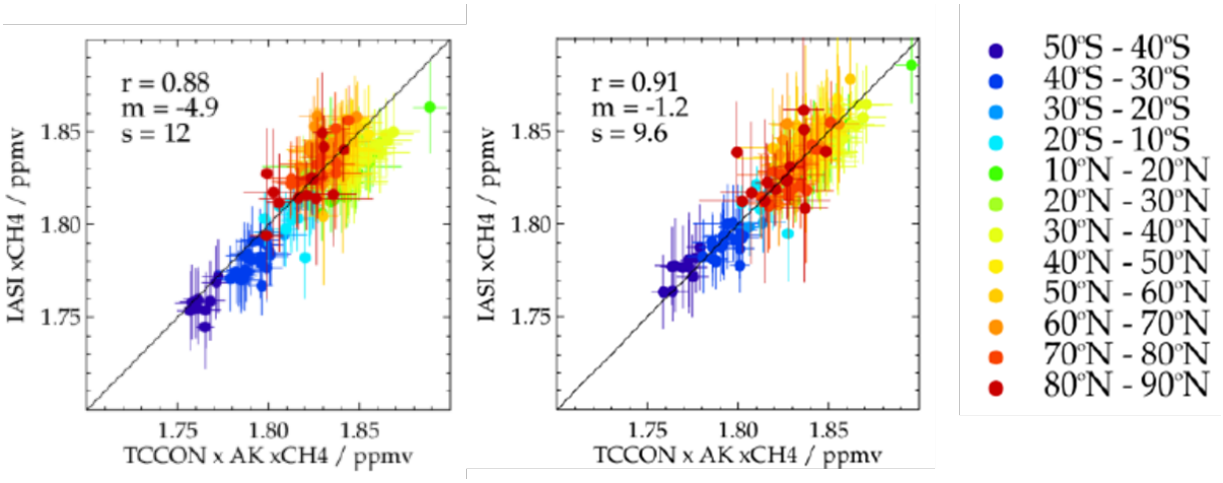

Figure 10: Scatter plots comparing IASI (RAL Methane+ V1 and V2) column average methane mixing ratio and TCCON (corrected for IASI vertical sensitivity using the averaging kernels). Left-hand panel shows V1 data; right-hand panel shows V2 data. Error bars in the plot indicate the standard deviation in the difference between individual retrievals and TCCON in the given month. Figures in each panel show the correlation of the monthly mean values ("r"), mean difference ("m") and standard deviation in the monthly mean values ("s"), with the latter two being in units ppb.

An extensive series of tests was undertaken to identify and mitigate some of the issues found in the V1 data. This resulted in the following modifications to the scheme (see [CH4+ ATBD TIR]):

1. Modelling of the N_2O profile was improved using new SCISAT ACE-FTS data.
2. The prior constraint on methane was relaxed, by adding correlated errors to the prior covariance, such that the retrieval is free to scale the whole methane profile, as well as adjust the profile shape.
3. The spectroscopy underpinning the RTTOV model was updated, including modelling of line mixing. This enables the complete fit window from 1232.25-1290 cm^{-1} to be used, without omitting spectral gaps known to be affected by line mixing. RTTOV was updated from V10 to V12, enabling improved modelling of cloud and aerosol (see below).

Tests indicated that using a wider spectral range, up to 1335 cm^{-1}, would add more information on the methane profile (by including stronger methane lines), but could not be done in practise as fitting errors became too large. This was attributed to limitations in the spectroscopic data and/or line modelling (even after this update).

4. Forward model errors were characterised as a function of column water vapour.
5. A new version of the IMS scheme "IMS-extended" was used to define temperature and surface spectral emissivity. IMS-extended exploits new features of RTTOV v12 to implement a more sophisticated approach to model cloud and aerosol compared to the original IMS scheme. This includes fitting sulphuric acid aerosol which is also input and modelled by the CH_4 scheme (expected to mitigate the impact of this aerosol on methane in volcanic plumes).
6. The methane scheme fits an offset, with linear spectral dependence, to the IMS-extended spectral emissivity. Surface temperature is no longer retrieved but is defined by the output of IMS-extended.
7. The IMS-extended approach to modelling cloud (as scattering layer rather than black-body), was adopted also in the methane scheme.
8. The digital elevation model (DEM) used in the extended IMS scheme and IASI methane module was updated (from GTOPO30 to GMTED2010).

As shown in Figure 6-9, the V2 data was generally found to agree better with CAMS, S5P and TCCON at lower latitudes and to show comparable agreement at higher latitudes at most times of year. I.e. there was a considerably smaller negative bias at low latitudes and weaker latitude dependence in the V2 data, together with reduced standard deviation in zonal mean differences, and reduced dependence on view zenith angle. Use of the improved DEM eliminated the anomaly over Venezuela. Retrievals over the desert were also generally improved by the modified approach to fitting surface emissivity / surface temperature. However, the V2 improvement was less clear for the ATom-4 and AirCore comparisons and, particularly, at high latitudes in winter compared to CAMS.

The importance of the stratospheric methane distribution to the column average increases at high latitudes where the tropopause is lower and, in Antarctica, surface elevation is higher. Column and layer average methane distributions in the CAMS flux inversion depend also on how well transport of methane from lower latitude sources and surface emissions within the Arctic are represented. The validation of CAMS at these latitudes/times of year is also limited by the lack of independent observations (in particular ones depending on sunlit observing conditions). It is therefore possible that the CAMS fields used as reference are less accurate at high latitudes. On the other hand, extremely cold surface temperatures and the spectral emissivities of snow and ice make TIR retrievals challenging at polar latitudes. The larger positive anomalies found there for V2 data could therefore be attributable to inadequacies in either the retrieval and/or CAMS.

Because of these issues, it was concluded that further R&D to improve the RAL TIR retrieval scheme was needed before fully re-processing the IASI mission (outside the scope of the current study). Topics identified for attention (in the Scientific Roadmap [CH4+ SR]) include:

- Implementation of improved spectroscopic line data anticipated from another ongoing ESA study. Improved accuracy of methane line parameters including line mixing is expected to: improve spectral fitting accuracy; reduce the need to fit a systematic residual spectrum and enable spectral coverage to be extended to strong methane lines to improve resolution of lower and upper troposphere layers and UTLS retrieval accuracy.
- Further diagnosis of specific conditions giving rise to apparent positive bias at higher latitudes between V2 TIR retrievals and some correlative data sets.
- Improve handling of marine low cloud / temperature inversions, which can lead to artefacts in continental outflow regions e.g. off Californian coast.
- Assess other remaining issues leading to land-sea discontinuities, not explained by vertical sensitivity.
- Assess/improve handling of cold surfaces to improve accuracy in the Arctic, Antartica and over sea ice where photometric precision is low due to cold surface temperatures.
- Investigate further parameterisation of spectral patterns used to mitigate forward model/instrumental errors (beyond the current dependence on view zenith and water vapour column), e.g. as a function of surface temperature or air/surface temperature contrast.

2.3.2. LMD IASI-B data product

LMD provided the reanalysed time series of IASI-B Mid-Tropospheric content of CH_4 version 9.1 from IASI-B observations for the period 2018-2020. The LMD CH_4 retrieval is based on a non-linear inference scheme based on neural networks (Crevoisier et al., 2009a, 209b, 2013). The inputs of the neural networks are a selection of simultaneous observations of AMSU and IASI instruments onboard Metop-B. AMSU channels are mainly sensitive to the temperature profile and the selected IASI channels are sensitive to both methane and temperature. By using them simultaneously, the information related to temperature can be decorrelated from that related to methane. In the end, the IASI-B LMD CH_4 product is a mid-tropospheric content of methane, denoted MT-CH_4 (Figure 11). It is the official IASI Level-2 product, but is not yet fully delivered by EUMETSAT (averaging kernels are missing).

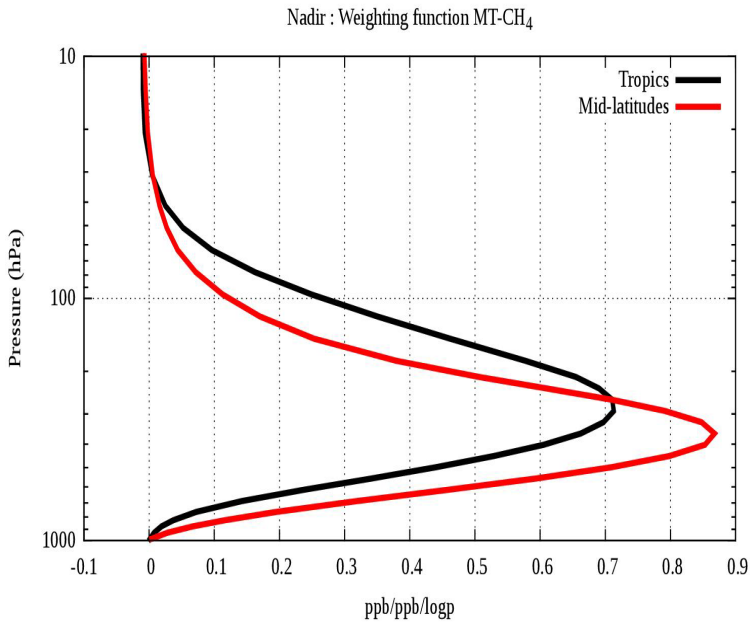

Figure 11: Example of averaging kernels of LMD IASI MT-CH4 retrievals

The retrievals are performed during day and night, and over land and sea. For each surface type (land or sea), for 7 surface levels, and for each of the 30 AMSU viewing angles, there is a specific neural network.

IASI-B MT-CH_4 has been compared to CH_4 profiles from dozens of AirCore acquired as part of the French AirCore program (https://aircore.aeris-data.fr), extrapolated with CAMS profiles and convoluted with the IASI-B MT-CH_4 averaging kernels. (An example of AirCore methane profile is given in Figure 12.) These comparisons show an average difference of -0.91 +/- 14.51 ppb (Figure 12). This result is consistent with the one obtained over the whole period of IASI/Metop-A and IASI/Metop-B (1.97 ± 12.94 ppb) (as shown in the C3S validation report for the LMD IASI v9.1 dataset, Buchwitz et al., 2020). Furthermore, The LMD IASI-B MT-CH4 has been validated using the Atmospheric Tomography Mission (ATom, Wofsy et al., 2018) extrapolated with CAMS profiles. In Figure 13 it can be seen that over the Tropics (where the tropopause is higher), we obtain good statistics with ATom, with mean differences close to 0 ppb and a standard deviation around 13 ppb; over mid-latitudes, we obtain biases close to 10 ppb (and a standard deviation close to 20 ppb), which might be due to extrapolation with CAMS, as illustrated in Membrive (2016).

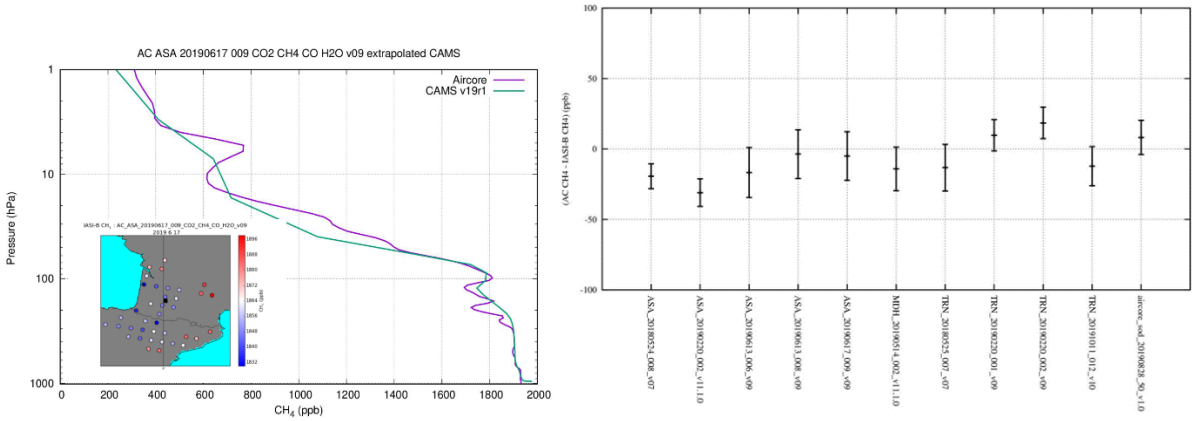

Figure 12: On the left, an example of a methane profile extrapolated with CAMS v19r1, from AirCore launched at Aire-sur-l'Adour, France; on the right, the comparisons between the IASI-B LMD MT-CH4 product and the CH4 obtained with the AireCore profiles convoluted with the IASI-B LMD MT-CH4 averaging kernels.

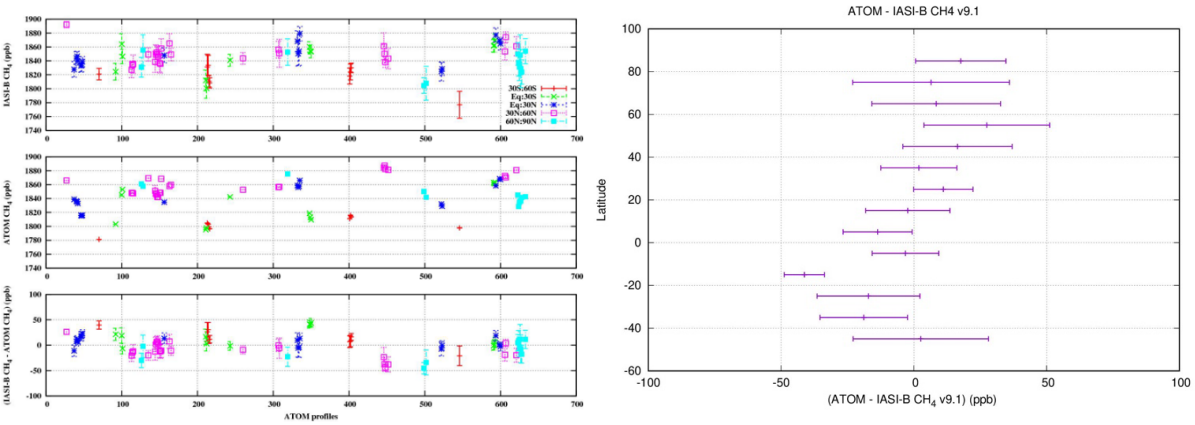

Figure 13: On the left: comparison in terms of MT-CH4 between IASI and ATom extrapolated with CAMS v19r1 profiles. (Top) IASI-B MT-CH4 for all ATom flights. (Middle) ATom-CAMS MT-CH4. (Bottom) Difference between collocated IASI-B and ATom-CAMS data. The colors indicate the latitudinal band where the IASI/ATom matches are located. On the right: differences between IASI and ATom extrapolated with CAMS v19r1 profiles against the latitude of the IASI/ATom matches. Horizontal lines show the standard deviation of the individual profiles about the mean difference.

Comparisons between the LMD IASI-B MT-CH_4 and CAMS v19r1 CH_4 profiles convoluted with the averaging kernel of LMD IASI retrievals have been performed (Figure 14). In terms of global difference distributions, the differences between CAMS and IASI are close to -5 ppb over the Tropics and, over mid-latitudes, around 5 ppb (with a maximum peak of around 15 ppb during Oct-Nov-Dec over northern mid-latitudes). The times series between IASI and CAMS are in good agreement, especially over Asia, China/India, Sahara/North Africa.

An independent study funded by EUMETSAT at the time of Methane+ has highlighted the very good performance of LMD IASI retrieval, with the exception of high latitudes, in agreement with the user warning not to use the data north/south of +/- 65°. Specific work will be needed in the future to improve the retrievals in this region, as northern high-latitudes areas are particularly important for methane. The study highlighted that the LMD IASI MT-CH_4 product reproduces the main features of CH_4 well (trend and seasonal variations).

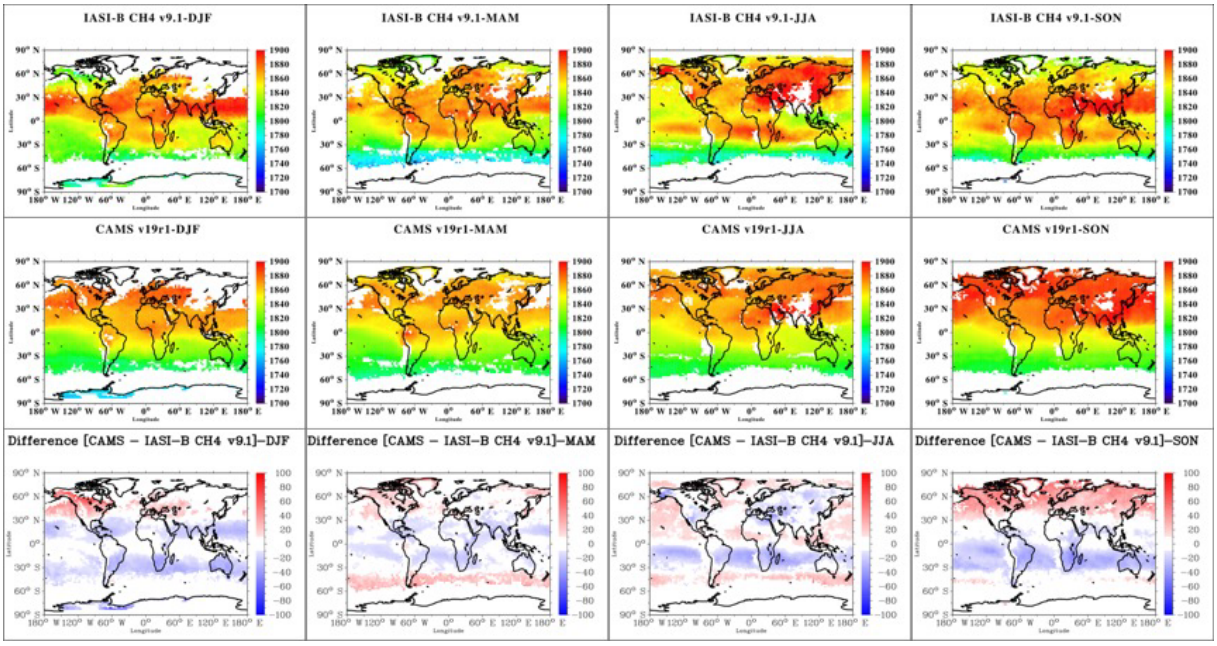

Figure 14: Global mid-tropospheric columns of MT-CH4 retrieved from IASI Metop-B: Each column of the figure shows results for a different season; December, January and February; March, April and May; June, July and August; September, October and November. The first and second rows show, respectively, results from IASI retrievals and CAMS v19r profiles with IASI averaging kernels applied. The third row shows differences between CAMS and IASI MT-CH4.

2.3.3. RAL CrIS Data Product

The RAL Methane+ V1 scheme was adapted to process data from CrIS on Suomi-NPP (S-NPP). Full spectral resolution CrIS L1B (version2) data from NASA GESDISC archive were used. In principle, S-NPP CrIS is better suited to use in combined SWIR-TIR retrievals with S5P because S-NPP is in a closely coordinated orbit with S5P (leading to a time difference of less than 5 minutes in observations). CrIS also provides 9 measurements per 50x50 km^2 field of regard compared to the 4 provided by IASI in a similar area. However, the (apodised) spectral resolution of CrIS is ~2.5 times coarser than that of IASI. This means that the information content for methane profile retrieval from individual CrIS soundings is significantly lower than for IASI. Example results from trial retrievals are shown in Figure 15. These show that the initial CrIS retrievals are generally biased low compared to IASI, particularly in the Tropics (exceeding the negative bias in the Tropics found in IASI V1 data).

Furthermore, the estimated error on the retrieved column average is much larger than that of IASI (typically 50 ppb for CrIS compared to 30 ppbv for IASI).

It should also be noted that a problem with the Suomi-NPP CrIS instrument means that there are no measurements in the spectral range used for methane retrieval for a period of approximately 3 months between March and June 2019. This would be a significant gap for the inverse modelling experiments conducted in Methane+, which focused on 2018-2020.

Given the retrieval limitations and considering the data gap, it was decided not to proceed further with CrIS in the Methane+ study and to prioritise IASI for both the SWIR-TIR combined retrievals and the inverse modelling experiments. This was a prioritisation which also reflected the time and resources available in the study. Further work to improve the CrIS retrieval remains valuable. In particular, the reduced information content of CrIS compared to IASI might be mitigated by widening the methane fit window: adding stronger methane lines is expected to add more profile information for CrIS than IASI, as the latter extracts more profile information from its finer spectral resolution. However, widening the spectral range is contingent upon having improved spectroscopic data (as demonstrated during the development of the IASI V2 scheme). The negative bias in CrIS could be mitigated through further work to diagnose the underlying cause, analogous to that carried out for the V2 IASI scheme. It would be logical to revisit CrIS after the planned further work for IASI is carried out.

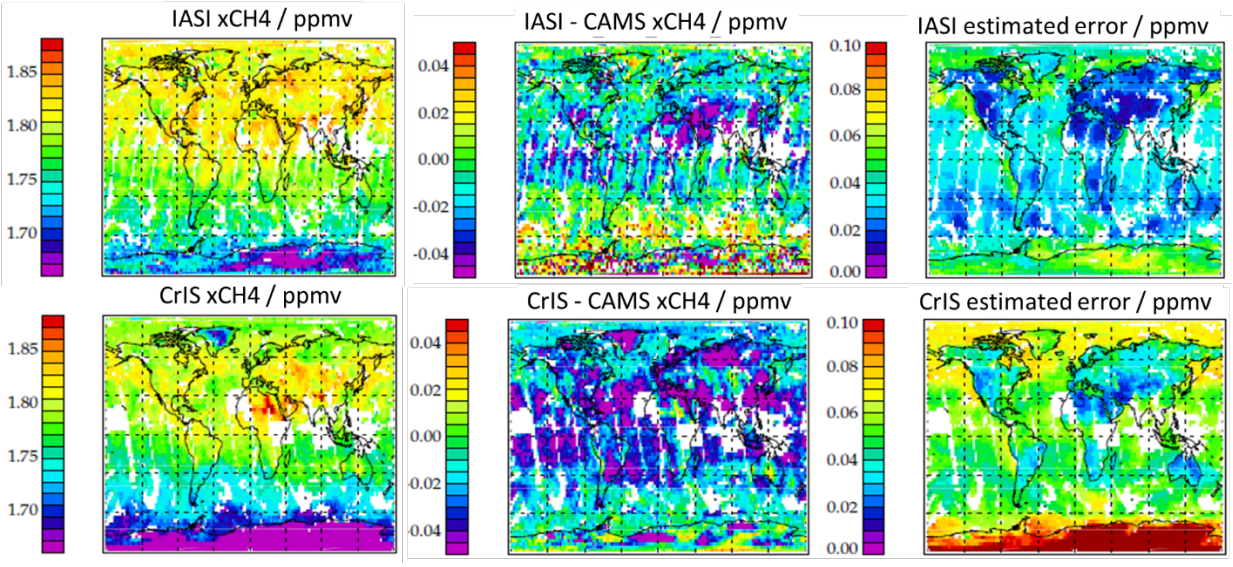

Figure 15: Comparison of Methane+ V1 IASI and CrIS data on 15 July 2018. Top panels show IASI; bottom panels show CrIS. Panels from left to right show the satellite column averaged methane mixing ratio; the difference between satellite and CAMS column averaged mixing ratio (accounting for averaging kernels); the estimated error on satellite column averaged mixing ratio.

2.4. TIR and SWIR combined data product

RAL's scheme to combine SWIR and TIR in the retrieval domain has been demonstrated for methane in this study with S5P and IASI V1 data, having first been developed and applied to S5P and CrIS CO data in Dr. Diane Knappett's Living Planet Fellowship[3].

The scheme uses an optimal estimation framework to combine independent SWIR and TIR retrievals (i.e. combining L2 data products). Details of the scheme are described in the joint scheme ATBD [CH4+ ATBD SWIR+TIR]. The objective of the SWIR-TIR combination is to resolve a lower tropospheric layer, exploiting the fact that the SWIR retrieval has sensitivity to the total column, while information from the TIR is limited close to the ground (due to the reduced thermal contrast of the lower atmosphere with respect to the surface). The joint retrieval scheme estimates a methane profile which is consistent with the two input retrievals, using their respective averaging kernels to characterise their vertical sensitivity, and taking into account their respective error covariances.

Data from March 2018 to March 2021 was produced using SRON S5P Version 18_17 data and RAL IASI-B Methane+ V1 data. The combination uses the column average measurement from S5P, combined with IASI sub-columns for the layers 0-6km, 6-12km 12-16km and 16km to top-of-atmosphere. Latitude- and time-dependent bias corrections, relative to CAMS, were applied to both S5P and the IASI product before the combination was performed. The combined retrieval was carried out for individual S5P scenes, using the nearest co-located IASI retrieval. This generally results in spatial coverage similar to that of S5P, only slightly reduced where no co-located IASI retrieval is found within 30km of the S5P pixel centre. (In general, cloud filtering is much stricter for S5P than for IASI, so it is almost always the case that an IASI retrieval can be co-located with an S5P scene.) The same IASI retrieval will tend to be combined with multiple neighbouring S5P retrievals. The joint retrieval outputs methane sub-columns in a layer corresponding to 0-2 km, as well as the sub-columns reported by the TIR-only scheme (0-6, 6-12, 12-16 km etc.).

Global, seasonally-averaged results (combining data in 2018-2019) are shown in Figure 16. In general, the column average from the combined retrieval (not shown) is found to follow S5P very closely and the 6-12 km layer tracks IASI, albeit less closely. This behaviour is as expected and reflects the different vertical sensitivities of S5P and IASI. In combining with S5P, the number of degrees of freedom for the IASI-only retrieval is typically increased from around ~2 to 2.5-2.8. Lower tropospheric layers are clearly influenced by both the S5P and IASI observations, and tend to show increased mixing ratios nearer to the surface, where S5P has positive anomalies (compared to the zonal mean) suggesting regions of methane surface emission.

[3] A full TIR v2 data set was not produced in this study and therefore neither was a SWIR-TIR data set based on TIR v2.

Distinctive, coherent positive anomalies are found for the 0-2 and 0-6 km layers over locations associated with methane emissions: the Indo-Gangetic plain, Bangladesh wetlands, Amazonia, South Sudan and the Central Valley in California, which are more pronounced than those in the S5P column average. The enhancements tend to be much stronger in the 0-2km layer than the 0-6km. Figure 17 shows an example over central Africa, in which a prominent enhancement detected by S5P over the Sudd wetlands is clearly (and realistically) placed by the joint retrieval in the 0-6km layer (and hardly noticeable in the 6-12km layer).

Other features in the combination are likely caused by retrieval artefacts (in TIR and/or SWIR input), however, and these also tend to be more pronounced in the 0-2 km layer than in the 0-6 km layer and higher. This is partly consistent with the larger error in the 0-2 km layer estimated by the retrieval itself. Recognising that these retrieval artefacts seemed to particularly affect the 0-2 km layer, it was recommended to use the 0-6 km layer in inverse modelling tests with the new combined data product.

On the basis of this first application of the combination scheme, our finding is therefore that the SWIR-TIR combination does have potential to provide added value to SWIR column averages and TIR height-resolved data. Use of the IASI-B V2 data in place of V1 would provide greater accuracy at lower latitudes. Improvements implemented in the SWIR scheme during Methane+ would also remove some S5P related artefacts. However, further R&D to the TIR scheme would improve accuracy more generally at higher as well as lower latitudes. In addition, the SWIR-TIR scheme is itself amenable to improvement, e.g. through modification of the prior constraint.

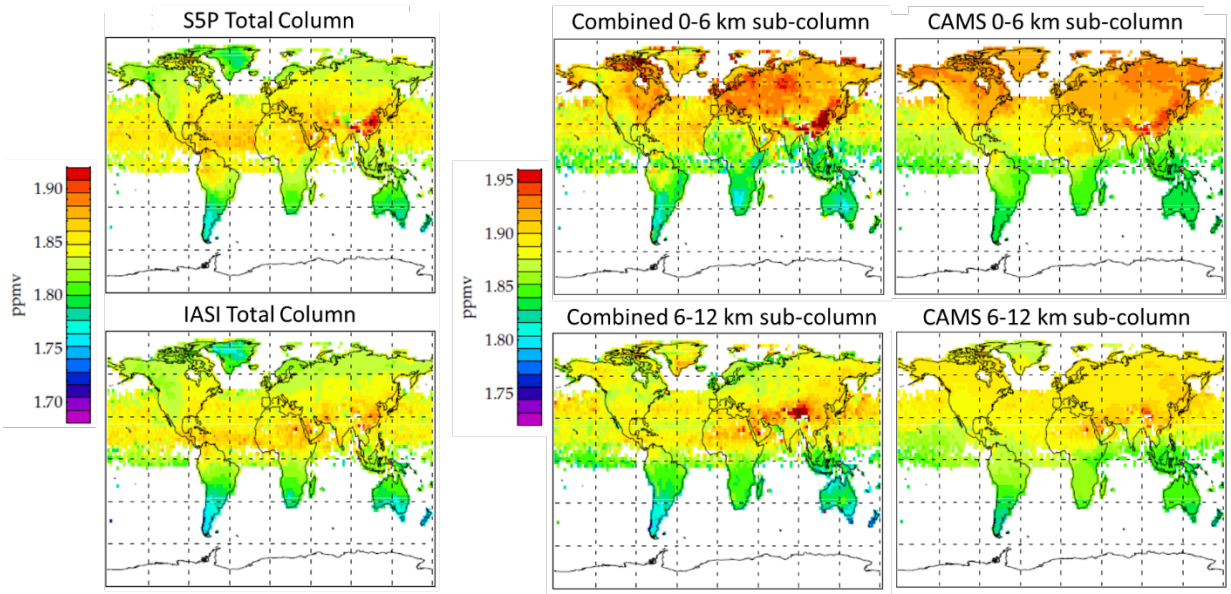

Figure 16: Illustration of global SWIR-TIR retrievals for June-July-August (2018-19 combined) at 2.5° x 2.5° spatial resolution. Panels on the left show the column-averaged mixing ratio from S5P (top) and Methane+ V1 IASI TIR-only retrieval (bottom). Centre panels show the SWIR-TIR retrieved sub-column averaged mixing ratio for the 0-6 km (top) and 6-12 km (bottom) layers. Right-hand panels show the corresponding sub-columns from CAMS.

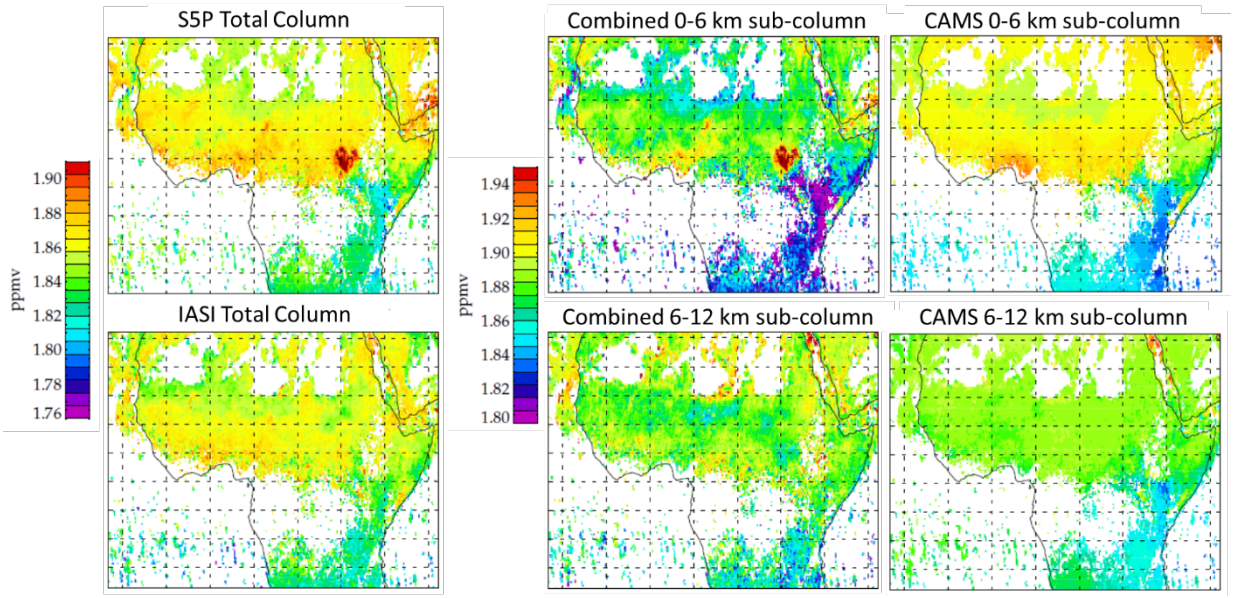

Figure 17: As previous figure, for the September-October-November seasonal average, at 0.5° x 0.5° resolution over central Africa.

2.5. Summary TIR and Combined TIR and SWIR

TIR methane data have been produced for use in Methane+ from 2018-2021, by both the RAL and LMD retrieval schemes.

Data from the V1 RAL optimal estimation scheme and the LMD non-linear inference scheme have been applied to Metop-B IASI through 2018 and 2019. The products have been validated on a common basis, applying vertical averaging kernels, with co-located profiles from the ATom-4 campaign and AirCore launches over France and Sodankylä. Data have also been compared to the CAMS flux inversions v19r1 using global and regional seasonal maps and Hovmöller plots. Column averages from the RAL scheme have been compared in addition with those from TCCON and Sentinel-5P. Results for the RAL (V1) and LMD data from these analyses for Metop-B are found to be similar to those from earlier analyses for Metop-A.

LMD coverage is generally limited to latitudes 60° S – 60° N except in northern summer due to strict quality filters. Fundamental differences in retrieval methodology and spectral sampling mean that the vertical sensitivity of the LMD mid-troposphere column (MT-CH_4) differs from that of the RAL column average, surface-450 hPa (0-6 km) and 450-170 hPa (6-12 km) layers. This in turn means that global and regional maps and Hovmöller plots would not generally be expected to show a consistent structure, nor would their comparisons with CAMS. This is evident from CAMS global and regional maps with respective averaging kernels applied for the LMD MT-CH_4 and RAL (V1) column and layer averages. Global and regional maps for the different layers retrieved by the RAL scheme, and their deviation from CAMS, exhibit significantly different structure. The RAL V1 column average is generally within +/-20 ppbv of CAMS and the LMD MT-CH_4 within +/-40 ppbv, with the highest deviations at high latitudes. In cases where CAMSxAK maps are similar for RAL column average and LMD MT-CH_4, there is an indication that latitude-dependent biases with respect to CAMS are different: negative at low latitudes and positive at high latitudes for RAL and vice versa for LMD MT-CH_4. Overall, RAL V1 column average and LMD MT-CH_4 retrievals both exhibit small biases with respect to ATom-4 profiles and AirCore profiles. Given the different vertical sensitivities and comparable levels of agreement with ATom-4 and AirCore profiles found for RAL column and layer averages and LMD MT-CH_4, the RAL V1 data could be expected to add value to LMD data in the CAMS assimilation system once a bias correction has been applied.

On the basis of this analysis and further investigation of artefacts e.g. low emissivity areas of Sahara and a topographic feature in southern Venezuela, improvements were made to the RAL scheme, resulting in a “candidate” V2 dataset. The V2 data show a substantial reduction in negative bias at lower latitudes, but mixed results at higher latitudes, with a larger positive bias particularly in winter/spring. It was therefore decided not to proceed with a full-scale reprocessing with the new scheme until further work is conducted to address the remaining issues (outside the scope of the current study).

Application of the RAL scheme to CrIS produced some promising results, but with generally larger negative bias than IASI in comparison to CAMS, and less height information due to the lower spectral resolution of CrIS. Although not prioritised in this study, further work to address these limitations in the current CrIS retrievals is recommended for the future.

Joint SWIR-TIR retrievals (based on S5P and RAL V1 IASI data) have also been produced during the project. This first attempt at the SWIR-TIR combination clearly shows promise, in placing near-surface emission features detected by S5P in the lower layers of the atmosphere, while upper layers follow structures from the TIR retrieval. Results are limited by the quality of the input retrievals and it is expected that the improvements to the S5P and IASI V1 data demonstrated by this project (and expected from future work) will lead to high-quality joint retrievals in the short to medium term.

Looking ahead, co-located SWIR and TIR measurements to be made by S5 and IASI-NG on MetOp-SG offer an ideal opportunity to exploit the potential of the SWIR-TIR approach to monitor methane in the lower troposphere from the mid-2020s onwards.

3. Inverse modeling WP3000

3.1. Introduction

This WP developed two inverse modelling systems, TM5-4DVAR and Jena CarboScope, for the use of the new satellite datasets from TROPOMI and IASI that were made available from Methane+ WP2000. Inversions have been carried out using these data to investigate the complementarity of the information on sources and sinks of methane that is provided by IASI and TROPOMI. This concerns mostly the different vertical sensitivity of the two instruments, due to their use of light absorption by methane in different wavelength regimes, dominated either by sunlight or emissions from the Earth's surface. Besides a different vertical sensitivity, this leads also to a different spatio-temporal coverage, as TIR measurements do not depend on the availability of sunlight. The impact of these difference on the ability to quantify methane sources and sinks using inverse modelling has been investigated by comparing inversions using data from either TROPOMI or IASI as well as their combination. In WP3000 this is done by comparing the global patterns of surface emissions that the inversions generate, as well as impacts in specific regions for which the vertical profile of methane and/or the seasonal data coverage is expected to be important.

An important short-coming of global methane inversions is their limited capability to attribute model-data differences to either surface emissions or atmospheric sinks. This is because the measurements represent the impact of both, in a way that cannot easily be deconvoluted in the inversion by accounting for atmospheric transport only. In the past this problem has been solved using either measurements of another tracer, such as methyl chloroform, which is sensitive to the same sink as methane but has well known sources, or by assuming that atmospheric sinks are stable and only solving for emissions. The latter approach is currently used by the CAMS reanalysis, even though the long-term trend in OH was found to be important enough to represent by simulations of a chemistry transport model. However, the uncertainty in model-simulated trends and interannual variations in OH is large, calling for the use of measurements instead. Since methyl chloroform emissions have been phased out under the Montreal protocol, its atmospheric abundance has dropped to levels that are difficult to measure and will soon no longer be useful.

The question we address in WP3000 is if the combined use of SWIR and TIR CH_4 retrievals provides sufficient independent information to estimate sources and sinks of methane independently.

3.2. Methods

We make use of the global inverse modelling systems TM5-4DVAR [Krol, 2005] and the Jena CarboScope [Rödenbeck, 2005]. These systems simulate global methane mixing ratios starting from a priori information on the global distribution of methane sources and sinks, based on emission inventories and process model output.

The simulated mixing ratios are compared to satellite data by sampling vertical columns of the modelled atmosphere in the same way as satellites sample the Earth's atmosphere. The mismatch between the model and the data is passed on to an optimization algorithm, which finds the most likely source and sink adjustments that bring the model in agreement with the data, taking the uncertainties in the prior fluxes into account. Further information about the inverse modelling systems is provided in the Methane+ Requirements Baseline Document [CH4+ RBD].

To prepare the inverse modelling systems for satellite retrievals from TROPOMI and IASI, model operation operators were implemented that sample the model according to the locations and vertical sensitivities of the satellite retrieved total columns. The comparison between model and measurements needs to account for model and measurement uncertainties as well as any systematic differences that may arise from model or retrieval deficiencies. The latter includes a latitudinal bias correction (see Figure 18) that is needed to ensure that optimal fits to satellite data are also consistent with measurements from the surface monitoring network.

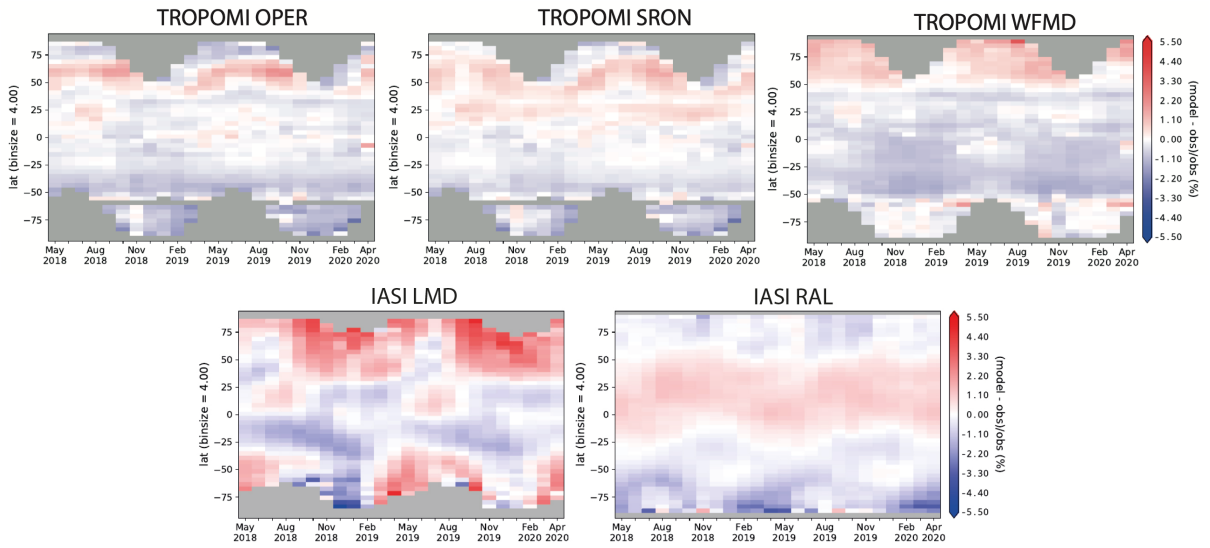

Figure 18: Seasonal and latitudinal bias between satellite data and TM5-4DVAR optimized using surface data used for bias correction.

The TROPOMI bias corrections show patterns that are similar between retrieval versions, which is caused most likely by the representation of the stratosphere in the TM5 model. In the case of IASI, important differences are seen between the LMD and RAL retrievals which must be in large part due to the retrieval.

The implementation of the bias correction in the Jena CarboScope was performed slightly differently, using a second-order polynomial fit by month and latitude following Bergamaschi et al. (2007). This bias correction was implemented as an additive factor rather than a multiplicative correction. As a sensitivity test, both approaches were compared within the Jena CarboScope, but found to not significantly affect the results (as reported in [CH4+ SAR]).

Within the Jena CarboScope, the bias corrections for the thermal infrared products were found to be unrealistically large, suggesting fundamental problems with the representation of the methane gradients around the tropopause in the TM3, which are inconsistent with what is measured by IASI. Further details about the implementation of satellite data in TM5-4DVAR and Jena CarboScope can be found in Methane+ WP3000 report [CH4+ SAR].

The TM5-4DVAR inversion system has been modified for the optimization of hydroxyl radical sink. The inversions that were performed using this extension solve for global annual scaling factor of the a priori OH field that is used in all TM5-4DVAR inversions. The setup has the flexibility to increase the number of latitudinal bands and time intervals that are used to optimize OH. The implementation of OH sink optimizations includes the required modifications of the adjoint model, as explained in further detail in Methane+ WP3000 report [CH4+ SAR].

3.3. Global results comparing inversions and datasets

Inversions have been performed for a 2-year and 3-year time window (see Table 2). The 2-year inversions are used to evaluate the impact of differences between retrieval techniques on inversion-estimated fluxes. The 3-year inversions extend to cover the full year of 2020 and are meant to investigate the causes of the strong methane increase that has been observed in that year. The 3-year inversions also test the impact of optimizing sinks and the combined use of TROPOMI and IASI data.

Table 2: Inversions performed in WP3000.

Retrieval dataset	Time window	Inverse model	OH optimization
Surface network	201801 - 202006	TM5-4DVAR & CarboScope	-
S5p Operational	201801 - 202006	TM5-4DVAR & CarboScope	-
S5p SRON v16_14	201801 - 202006	TM5-4DVAR & CarboScope	-
S5p WFMD v1.2	201801 - 202006	TM5-4DVAR & CarboScope	-
IASI LMD v9.1	201801 - 202006	TM5-4DVAR & CarboScope	-
IASI RAL v2	201801 - 202006	TM5-4DVAR & CarboScope	-
Surface network	201801 - 202103	TM5-4DVAR & CarboScope	+
S5p SRON v18_17	201801 - 202103	TM5-4DVAR & CarboScope	+
IASI RAL v2	201801 - 202103	TM5-4DVAR & CarboScope	+
S5p SRON & IASI RAL	201801 - 202103	TM5-4DVAR & CarboScope	+
Joint SWIR/TIR retrieval	201801 - 202103	TM5-4DVAR & CarboScope	+

3.3.1. TM5-4DVAR

This section presents results that have been obtained using TM5-4DVAR. A comparison of emission estimates from the 2-year inversions is shown in Figure 19. The fluxes are expressed as annual fluxes and represent the mean over the time window of the inversion minus 3 month's spin-up and spin-down (i.e. the two-year period from 2018-04-01 until 2020-04-01).

All inversions reduce the emissions over south-east Asia, but to a varying extent and with a varying attribution of this decrease between China and India. It is useful to also include the Middle East in this comparison. The Asian band of emission reductions is compensated by emission increases over the Tropics and the mid latitudes of the Northern Hemisphere. Regional differences occur, but the general pattern is fairly consistent between the inversions.

The surface inversion reduces emissions from China, India and the Middle East. All inversions increase the emission over the Middle East relative to the surface inversion, except for IASI RAL. The SRON TROPOMI retrieval shows less emission reduction over India and China than the surface inversions. Comparing the size of the adjustments with the a priori emissions in the top left panel it becomes clear that the adjustments represent a significant fraction of the total emissions over these countries. The IASI LMD inversion puts most of the emission reduction over China, whereas IASI RAL moves it westward to India and the Middle East compared with the TROPOMI inversion.

The inversions using TROPOMI and surface data increase the emissions over tropical lands (Indonesia, tropical Africa, tropical South America). This is less clear in the IASI inversions, which do not agree in the distribution between the three continents. Results for Europe and the USA are quite variable among all inversions. Note that the 2-year TM5-4DVAR inversions do not optimize the OH sink.

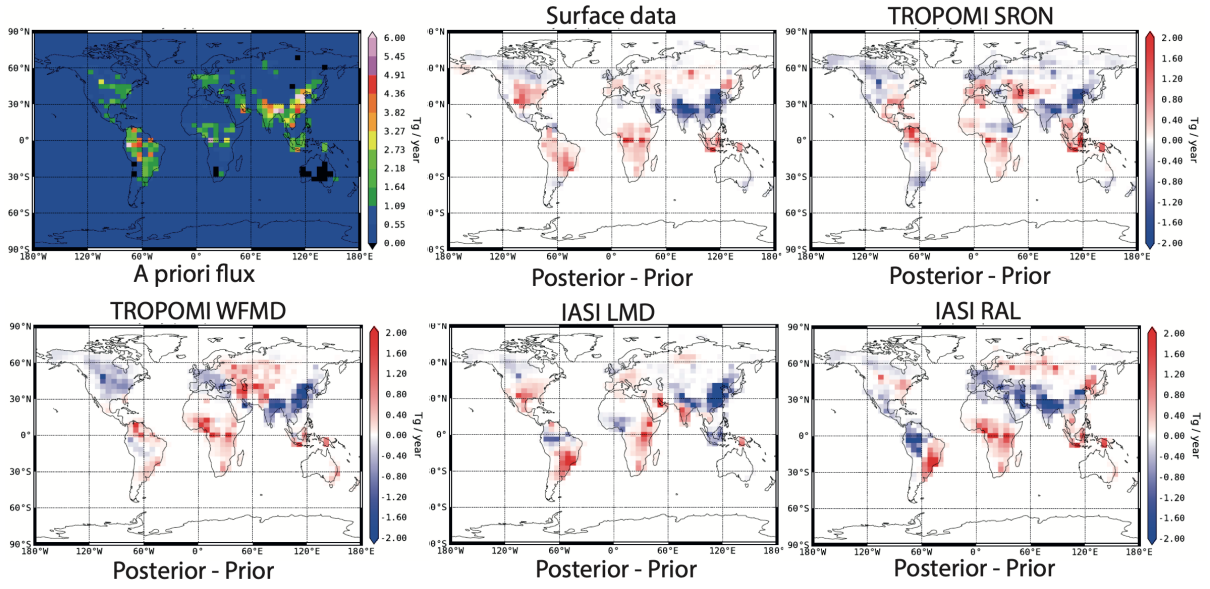

Figure 19: TM5-4DVAR optimized fluxes for inversions using different satellite datasets. Differences are shown between a posteriori and a priori fluxes (top left panel) representing the 2-year period of 2018-04-01 until 2020-04-01

Next, we exam the results of the 3-year inversions focusing on the difference between the flux estimates for 2020 and 2019. The estimated global totals vary substantially between inversions that use different satellite datasets (see Table 2).

A priori emissions are 11 Tg/yr lower for 2020 than for 2019, which can be explained by the reduced economic activity and associated reductions in the demand for oil, coal, and gas during the COVID-19 pandemic. To fit the observed growth rate acceleration in 2020 of about 5 ppb/yr (as reported by NOAA), the inversion can either increase the emission, decrease OH, or some combination of the two. As seen in Table 3, solutions are found using different satellite datasets that do not agree with any of these scenarios.

Table 3: TM5-4DVAR estimated global source and sink differences between 2020 and 2019

Inversion	Δ Global emission (Tg/yr)[#]	Δ OH sink (%)[#]
A priori	-11	0
Surface data	-4 (20)[$]	-8 (0)[$]
TROPOMI SRON	55 (25)	8 (0)
IASI RAL	6 (7)	-2 (0)
TROPOMI+IASI	33 (20)	5 (0)
Joint SWIR-TIR 0-6km	73 (22)	3 (0)

[#]: 2020 minus 2019; [$]: Results in parenthesis are for inversions that do not optimized OH.

Without OH optimization, a posteriori emissions increase between 20 and 25 Tg/yr, except for the IASI RAL inversion, which increases the emissions by only 7 Tg/yr. With OH optimization, the surface inversion transfers the emission increase of the inversion without OH optimization largely into a sink decrease. Other inversions, again with the exception of IASI RAL, find solutions that increase rather than decrease OH. Such solutions can increase the methane burden if the emissions increase even more, which is indeed what happens. The TROPOMI SRON inversion with OH optimization increases emissions by 55 Tg/yr (30 Tg/yr emission more than without OH optimization), while OH is increased by 8%. The extension of this inversion with IASI data in the TROPOMI+IASI inversions bring this solution in a more realistic range, with a 33 Tg/yr emission increase in combination with a 5% increase in OH.

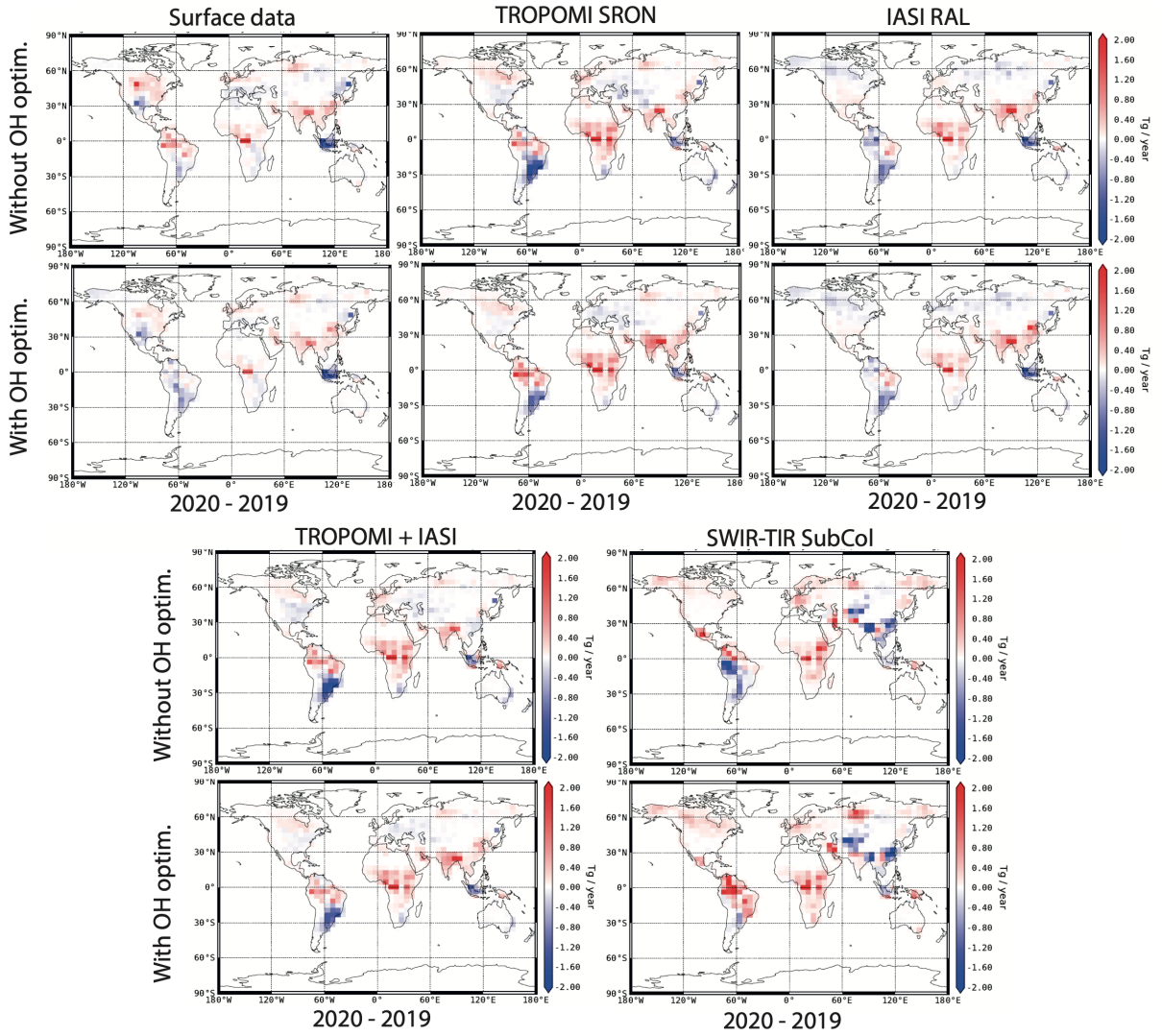

Figure 20: TM5-4DVAR optimized fluxes from 3-year inversions with and without OH optimization. Differences are shown between emissions for 2020 and 2019 for inversion using TROPOMI, IASI and combinations of them, with the inversion using surface data as reference.

To understand what might cause the varying solutions and increases in OH that seem inconsistent with an enhanced growth rate, we need to examine the spatial patterns of emission adjustment (Figure 20). The largest emission increases are found in the Northern-Hemisphere Tropics. Depending on the sign of the OH adjustment, this increase is large or small.

The location coincides with the latitudinal band where the largest impact of OH changes are expected. This is because OH levels are highest in the Tropics and because the Northern Hemisphere is most strongly influenced by anthropogenic emissions of air pollutants, and therefore by reduced emissions during COVID lockdowns. The trade-off between emission and sink adjustments in the inversion is probably driven by differences in the degrees of freedom that are assigned to them in the inversion setup.

Since the OH field is only adjusted by a global, annual scaling factor, there is no flexibility to adjust OH only in the Northern Hemispheric Tropics. Depending on the strength of the observational constraint on changes in this latitudinal zone, emission adjustments might be more effective than sink adjustments. To investigate if this mechanism could lead to the misattribution of a sink to a source, additional inversions will be needed in which the number of degrees of freedom of the sink is varied.

3.3.2. Jena CarboScope

This section presents results obtained from the Jena CarboScope inversion. The preprocessing of the TROPOMI and

We begin by examining the spatial pattern in the posterior fluxes, as well as the increment from the prior, for inversions using different datasets, presented in Figure 21. This can be broadly compared to the results from the two-year inversion results from the TM5-4DVAR in Figure 19, although the time periods do not overlap exactly, and the data products inverted are also not identical.

Nonetheless, some broad similarities emerge: The surface inversion with the CarboScope also show negative increments (a reduction in emissions) over China, as was seen in the TM5-4DVAR runs. This pattern is not as robustly visible in the other simulations however, with the exception of the WFMD inversion.

The flux increments across south America are broadly similar across all the remote sensing products, but are both smaller and differently distributed for the surface-based inversion. In this regard, the surface-based inversion with the Jena CarboScope.

Given the extremely large model-data mismatch found between the surface-optimized fields and the RAL IASI retrievals when deriving the bias correction (discussed in Section 3.1 and shown in [CH4+ SAR]), it is not entirely surprising that the inversion of the IASI-RAL retrieval resulted in unrealistically large increments. This result can only be interpreted as a failure of the model to represent and interpret the measured gradients in the upper troposphere-lower-stratosphere.

The poor performance of the IASI total column product makes the comparatively reasonable results from the 0-6 km sub-column from the joint SWIR-TIR retrieval all the more interesting. The spatial patterns in the resulting flux increments are rather consistent with those seen in the SRON retrieval, and the WFMD retrieval. Whether that is simply reflecting the information content of the SWIR columns in this joint product or rather improved information about the lower troposphere remains a topic for investigation.

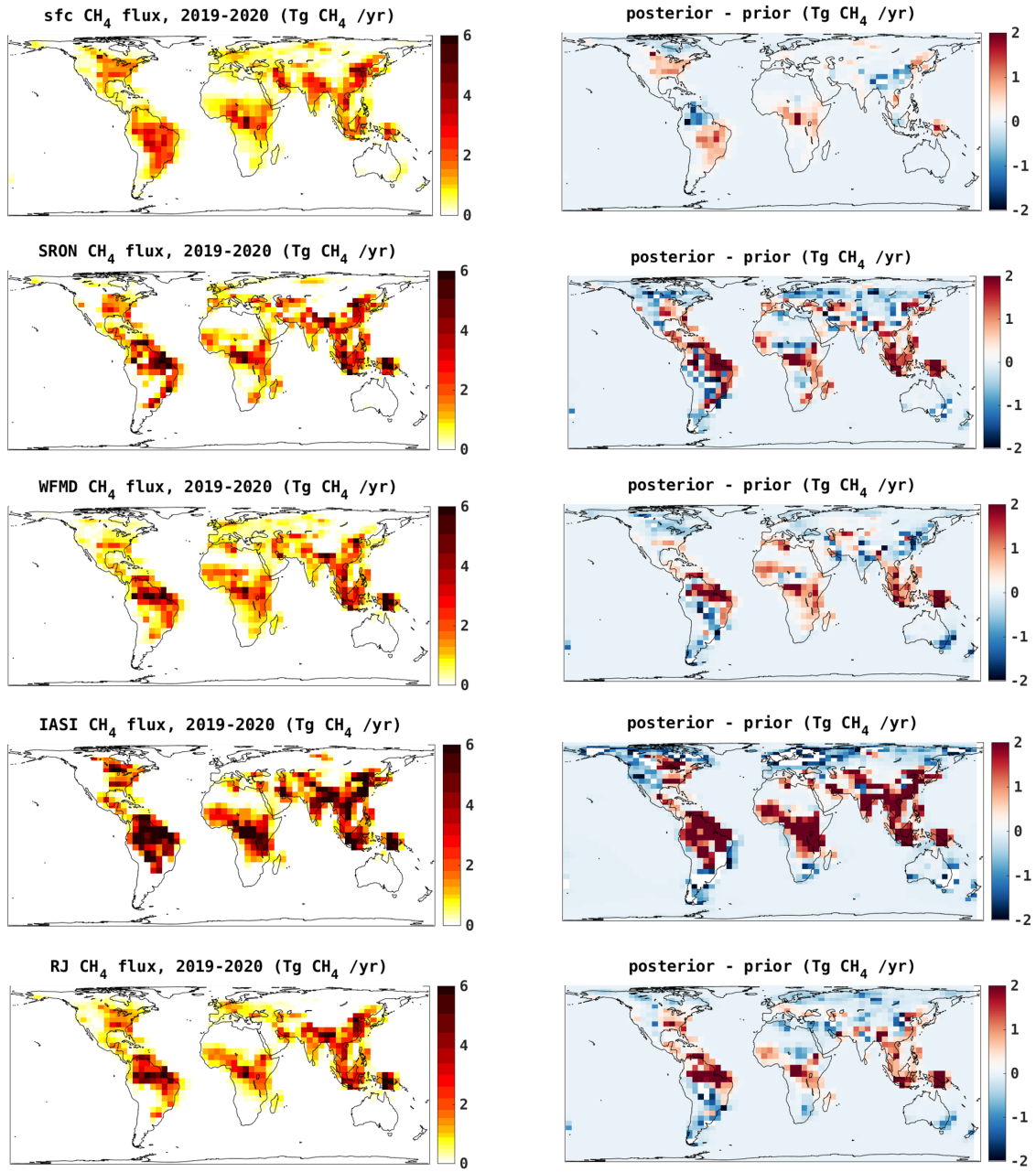

Figure 21: Posterior fluxes (left) and increments from the prior (right) using the Jena CarboScope for five different inversions, using different data constraints. From top: the surface-based network, the TROPOMI SRON retrieval, the TROPOMI WFMD retrieval, the IASI RAL retrieval, and the joint SWIR-TIR retrieval from RAL (labelled RJ here). The inversion period is from January 2019 through December 2020.

3.3.3. Inversion intercomparison

In this section the inversions are compared against in situ and ground-based remote sensing measurements. First, the performance of all TM3-4DVAR inversions have been assessed in comparison with the surface network, as shown for the 3-year inversions in Figure. Similar comparisons for the 2-year inversion (see the Methane+ WP3000 report [CH4+ SAR]) were used to test the implementation of satellite bias corrections. Figure 22 shows a comparable performance for most inversions, except for the joint SWIR-TIR 0-6km inversion. The cause of this is currently not clear. We were glad to be able to make a first attempt at inverting this data product within the timeframe of the Methane+ project, but the results call for a more detailed analysis of possible causes (e.g. the implementation of the averaging kernel, data filtering) than was possible over the course of this project.

Similarly, concentration fields from the Jena CarboScope inversions were compared against independent measurements from both TCCON (ground-based remote sensing instruments measuring XCH_4) and aircraft profiles. The results for the TCCON intercomparison are shown in Figure 23. From this plot it is clear that the two TROPOMI retrievals perform very similarly, which is encouraging. They also perform slightly better than the joint SWIR-TIR retrieval. In general, the data products including TROPOMI agree better with the TCCON data than the surface-based inversion, both in terms of having lower bias at most stations, and slightly lower standard deviation in model-data mismatch. This is not true for the few sites in the Southern Hemisphere however. In general, there appears to be an interhemispheric signal in model-TCCON biases, which is largest for the surface-based inversion. A similar shape was seen a comparison of the TM5-4DVAR results with TCCON (see Figure 21 of [CH4+ SAR]). The differences between the inversion results using the RAL IASI retrieval show such poor agreement (consistent with Figure 21) that they are often outside the plotted area. Similar results were found in the comparison of the Jena CarboScope inversions against independent aircraft-based profile measurements, except that the surface-based inversions outperformed the TROPOMI-based inversions in this case (not shown).

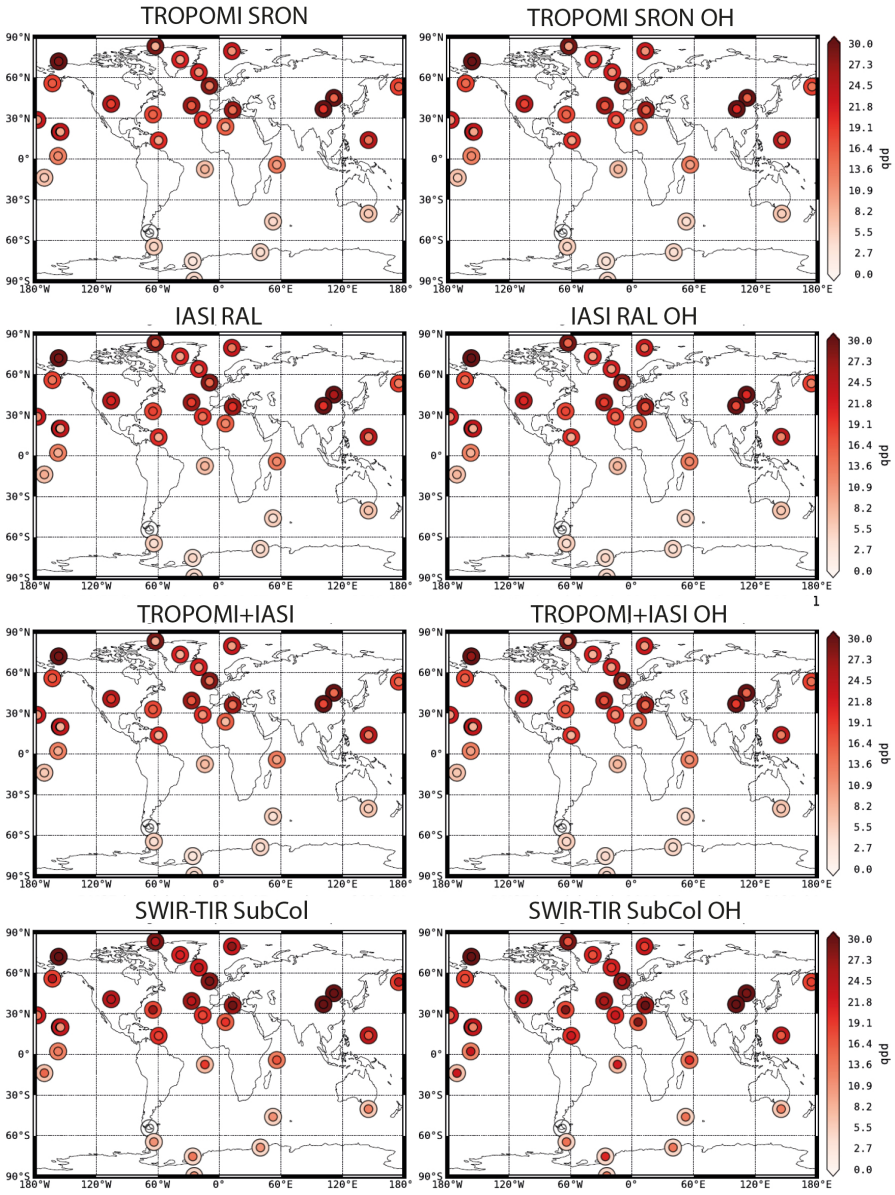

Figure 22: Fit residuals between TM5 and surface measurements for 3-year inversions. Outer rings represent the RMSE between measurements and the a priori model, inner circles that of measurements and the a posteriori model.

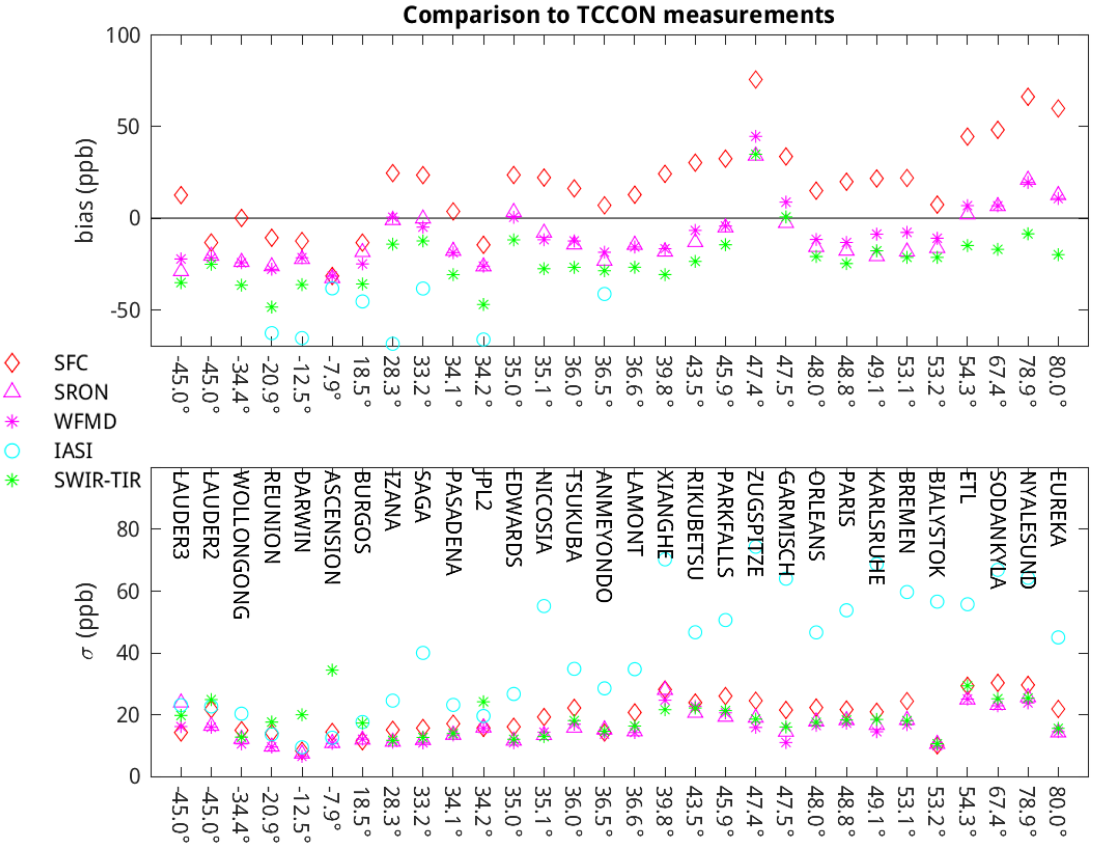

Figure 23: Comparison of TCCON measurements to different inversions with the Jena CarboScope. The upper plot shows the mean bias at each station, and the lower plot shows the standard devation of the model-data difference. The symbols are as described in the legend: red diamonds for the surface-based inversion, magenta triangles for the TROPOMI SRON retrieval, magenta stars for the TROPOMI WFMD retrieval, cyan circles for the IASI-RAL retrieval, nad green stars for the RAL joint 0-6km retrieval.

The comparison to independent aircraft-based measurements provides an interesting opportunity to compare the TM5-4DVAR results found with and without OH-optimization, which sometimes gave differing flux solutions, as seen in Table 3. These comparisons are summarized in Figure 24. Comparing the left and right sides of the plot (without and with OH optimization, respectively), it is clear that the results are quite similar by this metric. Upon closer examination, it can be seen that the bias below 6 km is generally a bit smaller for the simulations optimized OH fields, while above 6 km the reverse is true. However, these differences are small enough, that it cannot be conclusively said which result is more realistic.

Surprisingly, the inversion using the joint SWIR-TIR 0-6 km product from RAL agreed best with the aircraft measurements, both above and below 6 km. This is contrary to the result shown for the comparison to in situ stations in Figure 22, suggesting that the agreement for this inversion is poorer at the surface, but better throughout the rest of the atmosphere.

(Note that different metrics are used, with RMSE shown in Figure 22 vs. the mean bias and standard deviation of the residuals in Figure 24.) Regardless, it is clear that this inversion behaves differently from the rest, consistent with the results presented in Figure 20 and Figure 22.

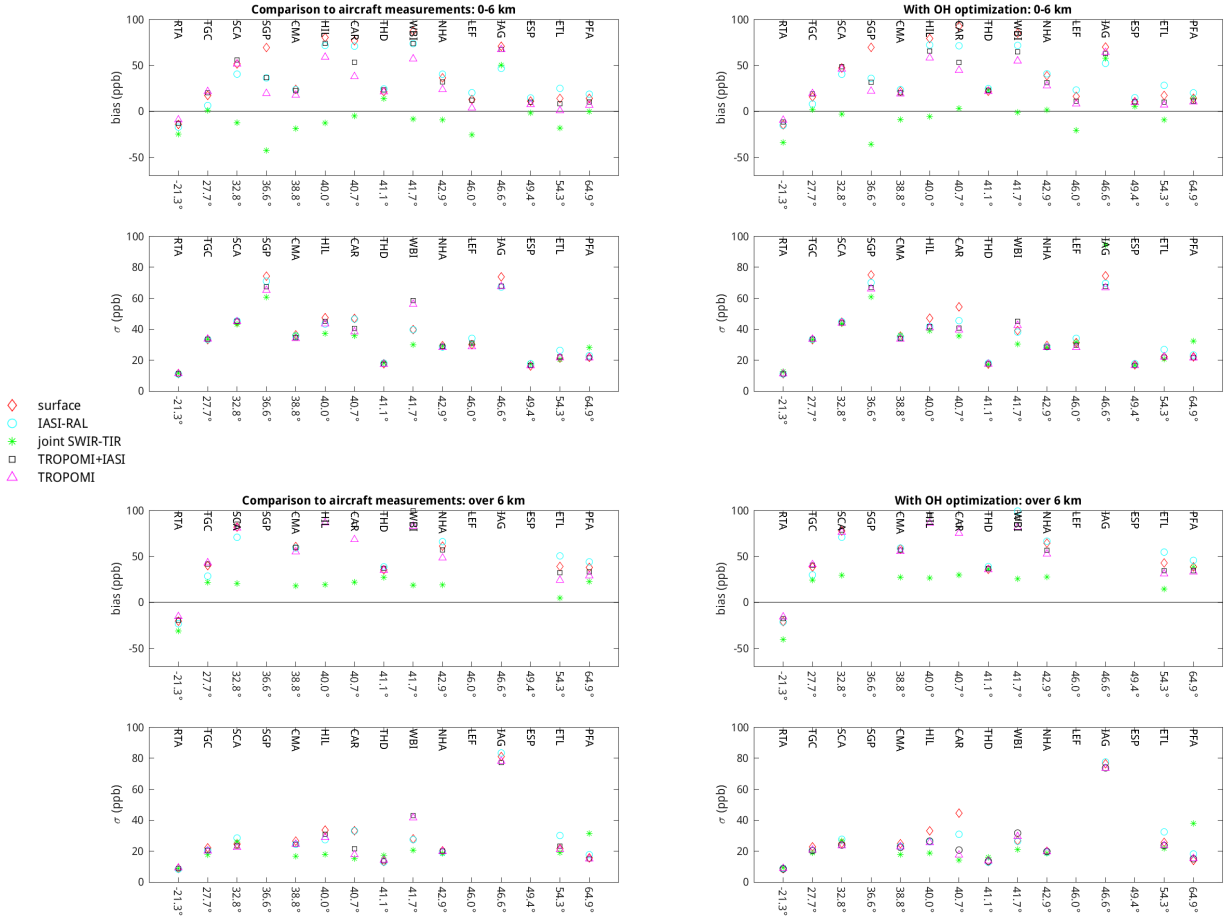

Figure 24: Comparison of TM5-4DVAR inversion results against independent aircraft measurements, with (right side) and without (left side) OH optimization. The top row of plots shows the bias and standard deviation for all aircraft data between 0 and 6 km, and the bottom row shows all data above 6 km. The symbols are as given in the legend, namely: surface-based inversion as red diamonds, IASI RAL inversion as cyan circles, the joint SWIR-TIR 0-6km retrieval as green stars, the separate assimilation of TROPOMI and IASI total columns as black squares, and the TROPOMI SRON inversion as magenta triangles. There were no data for SGP, LEF, or ESP above 6 km. The bias for IAG was outside of the plotted range above 6 km.

3.4. Benefits of combining SWIR and TIR CH4: case studies

Three regional cases have been analyzed in further detail to investigate the added value of combining SWIR and TIR retrievals. These are cases where information about the vertical profile of methane is expected to matter for a correct source attribution.

The first case study is the Indian summer monsoon, which injects a large amount of methane from low elevations into the free troposphere south of the Himalayas. In the upper troposphere, this methane is further transported by eastward and westward branches of the monsoonal circulation, respectively towards China and the Middle East. If only total column information is available, then methane enhancements over China and the Middle East originating from India could be misattributed to regional emissions by the inversion. Combining TROPOMI and IASI data could avoid this misattribution by constraining the contributions of the lower and upper troposphere to the total column.

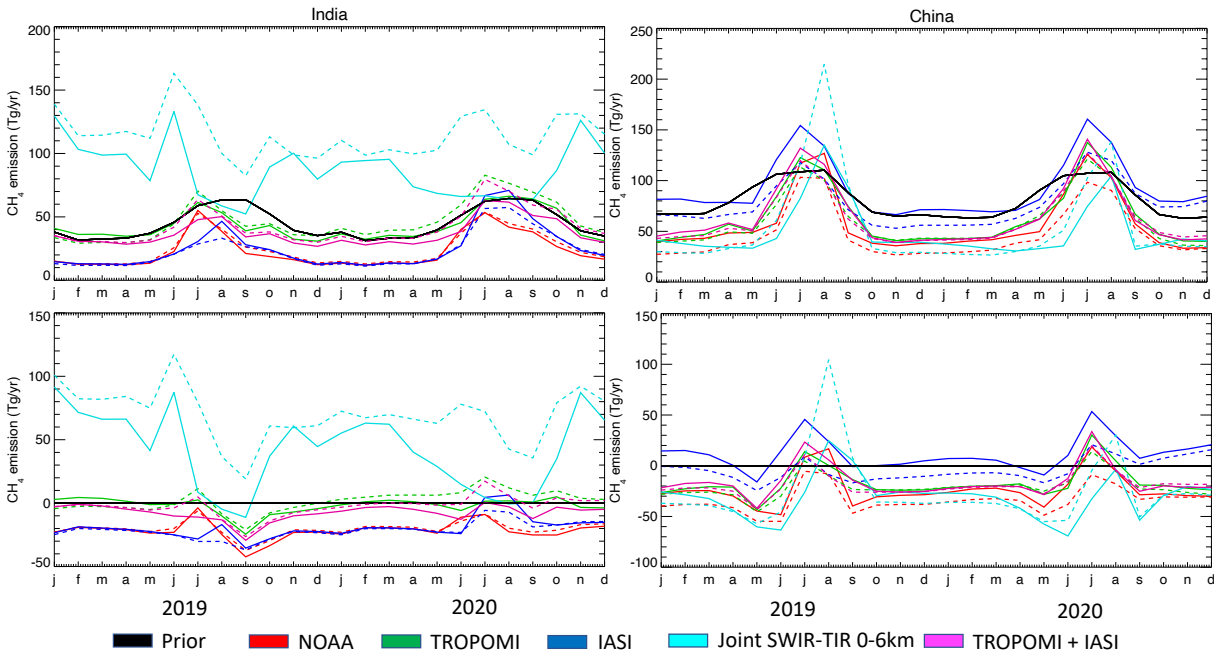

Figure 25: Region integrated fluxes over India and China. Dashed lines represent inversions that optimize OH. In the bottom panels the prior flux has been subtracted.

Monthly methane emission from TM5-4DVAR integrated over India and China are shown in Figure 21 for the 3-year inversions. On average, TM5-4DVAR reduces emissions over India and China compared with the prior. During the summer monsoon Chinese emissions are overestimated and Indian emission are underestimated compared with the prior, which is consistent with a transport-induced misattribution of emissions. Surprisingly enough, the inversion using IASI data, which mostly address the free troposphere, shows this most strongly.

The TROPOMI inversion stays closest to the prior for India, and close to the prior of China also during the monsoon season. Combining IASI and TROPOMI data in a single inversion yields a solution that is closest to the use of TROPOMI only. Hence, it can be concluded that the emission attribution to China and India is sensitive to the dataset that is inverted. It is not clear, however, if the use of IASI data, either alone or in combination with TROPOMI, improves the regional emission attribution.

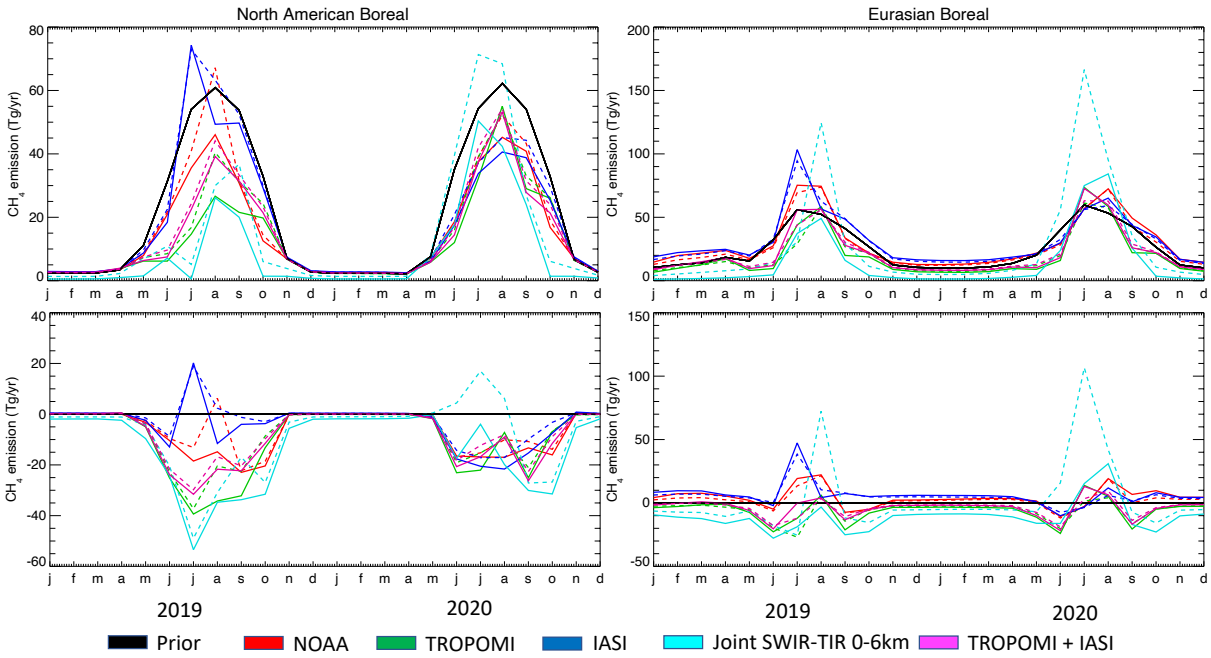

Figure 26: Region integrated fluxes over the northern high-latitudes. Dashed lines represent inversions that optimize OH. In the bottom panels the prior flux has been subtracted.

The second case investigates whether inversion-estimated methane emissions from high-northern latitudes are sensitive to the extended seasonal coverage of the high-latitudes provided by IASI in comparison to TROPOMI. Emissions are presented (see Figure 22) for Transcom regions North American Boreal, including Canada and Alaska, and Eurasian Boreal, covering the boreal/arctic zone of Eurasia east of the Ural Mountains. On average, the inversions reduce emissions over North America and increase emissions over Asia compared with the prior. All inversions agree on very low wintertime emissions over North America. Wintertime emissions are higher over Asia and highest using IASI data. Here the inversion using TROPOMI and IASI is more strongly influenced by IASI then in the previous example, which makes sense considering the year around availability of IASI data. The range of emission estimates is widest during summer – when observational constraints are strongest, but a priori flux uncertainties are largest also.

The last case is chosen over Tropical Africa and South America, where the XCH4 seasonality is driven by emissions from tropical wetlands and the movement of the Inter Tropical Conference Zone (ITCZ).

Again, the combination of TROPOMI and IASI could in theory facilitate the correct attribution of large-scale circulation (dominant at higher elevation) and regional emissions (dominant near the surface). The inversion estimated fluxes (see Figure 27 show increased emissions compared with the prior over equatorial Africa with the largest emissions from the NOAA and IASI inversions. Using TROPOMI, the emissions are least enhanced (disregarding the joint SWIR-TIR inversion). As for India and China, the impact of low vs high elevation retrieval sensitivity is opposite to the expectation. As expected, again, the inversion using IASI and TROPOMI data is in between the inversions using each of them. Over Tropical South America, the IASI emissions are lowest (and lower than the prior). Here, however, the deviations from the prior are not as strong – in relative sense – than over equatorial Africa.

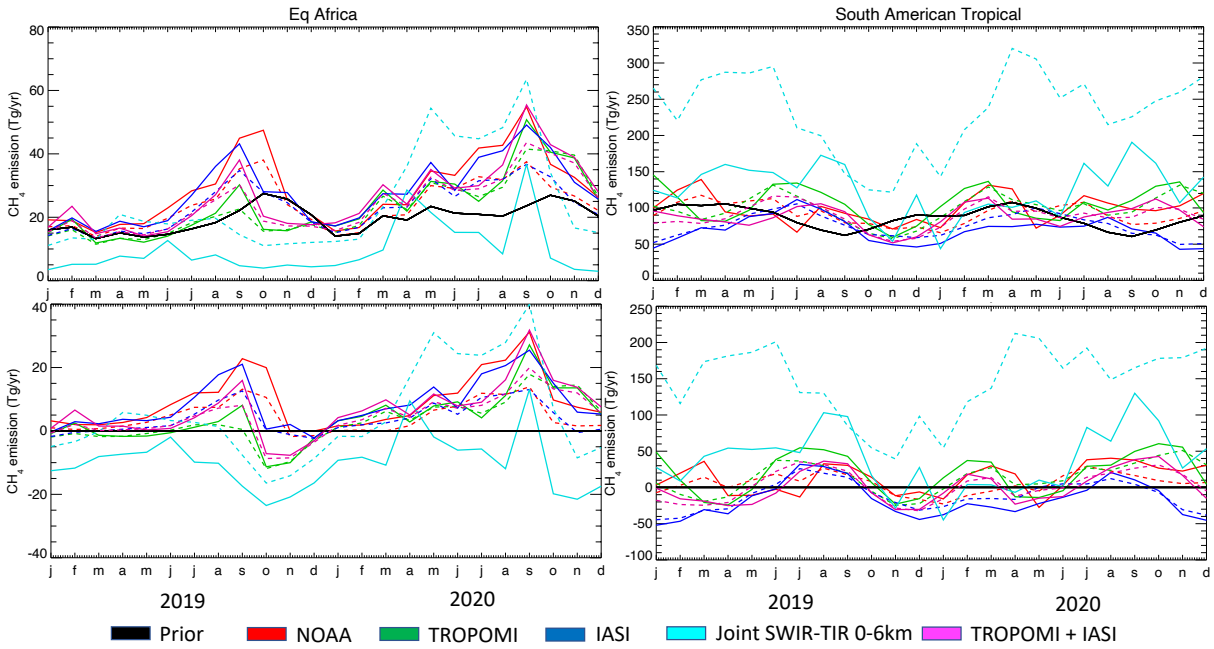

Figure 27: Region integrated fluxes over the Tropical rainforests. Dashed lines represent inversions that optimize OH. In the bottom panels the prior flux has been subtracted.

3.5. Summary results inverse modeling

The results presented in this section confirm that we succeeded in modifying the TM5-4DVAR and Jena CarboScope inversion systems for the use of the retrieval datasets that were made available by WP2000. The models are fitted to satellite data such that the consistency with the surface network is maintained. This is true for all retrieval datasets, including an inversion setup which combines TROPOMI and IASI data, but excluding the use of 0-6 km sub columns from the joint SWIR-TIR retrieval. The reason why the TM5-4DVAR inversion had difficulty fitting these data has not been elucidated yet.

The combined use of IASI and TROPOMI data to constrain a tropospheric sub-column is a promising approach because it avoids biases introduced by inconsistencies in the representation of the stratospheric sub-column. Therefore, it is recommended to continue the development of this retrieval product and its use in inversions, to solve the remaining issues.

Our inversions have been extended with one year beyond the 2-year period that was proposed initially to use the new satellite data to investigate the causes of sharp rise in global CH_4 that has been observed in 2020 and continued during 2021. This was also a useful test case for the extension of TM5-4DVAR with sink optimization capability, since OH changes during 2020 might have contributed to the accelerated methane increase. The difference between inversion optimized fluxes for 2019 and 2020 points to the northern hemisphere tropics having the largest contribution to this increase. Whether emissions increased or atmospheric sinks decreased cannot unambiguously be concluded from our inversions, as their relative contributions are sensitive to the dataset that is used.

So far, sinks have only been optimized using a single global and annual scaling factor. If global CH_4 sinks changed significantly due to changing emissions of photochemically reactive precursors of OH, such is NO_x, during COVID lockdowns, then this OH change is likely to have varied globally. In this case, additional degrees of freedom would be needed in the inversion to account for such changes. How to balance the degrees of freedom assigned to global methane sources and sink is a difficult question that requires further research. An easy next step would make use of output of CTM simulations that attempt to represent the change in OH. These OH fields could be optimized further or used to guide the choice of additional degrees of freedom for optimizing OH.

To further investigate the added value of combining SWIR and TIR data our analysis focused on regions where the vertical distribution of methane could be critical for a correct regional attribution of emissions. This was investigated for the influence of the Indian monsoon on inversion-estimated emissions from China and India, the influence and the seasonal migration of the ITCZ on the seasonality of emissions from tropical wetlands, and the seasonality of emissions at high northern latitudes. In the latter case, the advantage of combining SWIR and TIR lies mostly in the extended seasonal data coverage that TIR data can bring at high latitudes. The results of these regional analyses confirm that the optimized emissions are sensitive to the satellite dataset that is used. The combined use of SWIR and TIR data leads to solutions that are in between those of the separate datasets, with a balance between the two that can be explained by the weights of the constraints imposed by each of them. However, whether or not the use of more data leads to more realistic solutions cannot be concluded from the results that were obtained. While an initial validation using independent measurements was carried out (found in Section 3.3.3), no clear conclusion could be drawn. To better interpret the results, a more detailed evaluation using independent data is required, , which is also recommended as a next step.

4. Recommendations from Scientific Roadmap

4.1. Use of existing and upcoming missions

The main recommendations for activities on the short-term using existing data or preparing for the use of new data based on section 4 are:

- With TROPOMI an important step has been achieved in improving the SWIR XCH_4 measurement coverage. To make use of this capability to extend the quantification of methane emissions an additional step in retrieval accuracy is needed. In particular, the remaining dependencies on surface albedo need to be minimized.

- More realistic retrieval uncertainties are needed. To deal with the difficulty to quantify spatiotemporal uncertainty correlations, it is strongly recommended to use ensembles of retrievals methods developed by different research teams where available.

- Accuracy of the RAL TIR scheme was improved substantially at low latitudes in the Methane+ project, however, further work is needed to reduce positive bias at high latitudes, where surface temperature low, and other anomalies.

- The TIR and joint SWIR-TIR retrieval methods need to be developed further to improve their accuracy and vertical resolution, including use of new spectroscopic data when available and evaluation with ground-based measurements of the methane vertical profile as well as column average, and in preparation for MetOp-SG S5/IASI-NG.

- The optimization of CH_4 sinks developed in Methane+ should be improved further and tested using independent data.

- More effort is needed on global (and regional) inversion modelling to take optimal advantage of the new SWIR, TIR and joint SWIR-TIR datasets that have been developed in Methane+. Global inverse modeling frameworks need to be adjusted to deal with the higher spatial resolution, larger data volumes, and different sampling characteristics of the TROPOMI XCH_4 and IASI data products.

- Further research is needed to assess the benefits of using data from joint SWIR-TIR retrievals in comparison to joint use of data from the SWIR and TIR retrievals in inverse modelling.

- Further research is needed to identify the cause of the biases that are currently accounted for in an ad-hoc manner in inversions using SWIR and TIR satellite data. The evidence collected so far suggests that it is a model

problem, originating in the stratosphere. A dedicated research effort is needed focused on methane in the stratosphere, in cooperation with experts in stratospheric chemistry and dynamics.

- Further explore the use of existing satellites for detecting methane emissions from single facilities.

- Develop automated methods for efficient processing of large data archives on local methane emissions.

4.2. Requirements on future missions

Priorities for the development of future missions based on Section 4 are as follows:

- Improved year-round measurement coverage, with sensitivity to the planetary boundary layer, is needed at high northern latitudes, to support the monitoring of methane emissions from wetlands and thawing permafrost and their response to climate warming.

- The detection limit of high-resolution methane sensors to natural gas leaks has to be improved to be able to detect not only the largest emitters, but the leaks responsible for the main fraction of global emissions in the fossil fuel mining industry (on- and off-shore), as well as the main local sources in other sectors (e.g. waste management and agriculture).

- Support the ground-based validation network to help improve the accuracy of future satellite missions.

- Support the improvement of spectroscopy of methane and related radiative transfer modeling.

- Europe does not have a high (~20-200 m) spatial resolution methane satellite planned. Currently there is only a commercial satellite constellation (GHGSat) in space that measures methane at facility-scale resolution. CarbonMapper is a US-initiative to provide similar measurements for both CH_4 and CO_2. The DLR mission CO2Image, with 50-m spatial resolution is considering retrieving methane as a secondary mission objective, but this is still tentative.

- Support the development of atmospheric transport models operating at global, regional and local scales and inverse modelling methods that are used to translate satellite measurements into methane emissions and to disaggregate into different sectors.

References

Bergamaschi, P., et al., Satellite chartography of atmospheric methane from SCIAMACHY onboard ENVISAT: 2. Evaluation based on inverse model simulations, J. Geophys. Res., 112, D02304, doi:10.1029/2006JD007268, 2007.

Buchwitz, M., Crevoisier, C. and Armante, R., Product Quality Assessment Report (PQAR) – ANNEX E for IASI CO_2 and CH_4 (v9.1) and AIRS CO_2 mid-tropospheric products, project C3S_312b_Lot2_DLR – Atmosphere, v4.0, Ref: C3S_D312b_Lot2.2.2.3-v2.0_PQAR-GHG_ANNEX-E_v4.0, 2020.

Crevoisier C., Chédin A., Matsueda H., Machida T., Armante R. and Scott N. A. First year of upper tropospheric integrated content of CO2 from IASI hyperspectral infrared observations. Atmos. Chem. Phys., 9, 4797-4810 (2009a)

Crevoisier C., Nobileau D., Fiore A., Armante R., Chédin A., and Scott N. A. Tropospheric methane in the tropics - first year from IASI hyperspectral infrared observations. Atmos. Chem. Phys., 9, 6337-6350 (2009b)

Crevoisier, C., Nobileau, D., Armante, R., et al., The 2007–2011 evolution of tropical methane in the mid-troposphere as seen from space by MetOp-A/IASI, Atmos. Chem. Phys., 13, 4279-4289, 2013.

European Commission, The European Green Deal, COM(2019), 11 Dec. 2019.

European Commission, on an EU strategy to reduce methane emissions, COM(2020), 14 Oct 2020.

Froitzheim, N., Majka, J., Zastrozhnov, D.: Methane release from carbonate rock formations in the Siberian permafrost area during and after the 2020 heat wave, Proceedings of the National Academy of Sciences, 118, e2107632118, https://doi.org/10.1073/pnas.2107632118, 2021.

IPCC2013: Climate Change 2013: The Physical Science Basis. Contribution of Working Group I to the Fifth Assessment Report of the Intergovernmental Panel on Climate Change [Stocker, T.F., D. Qin, G.-K. Plattner, M. Tignor, S.K. Allen, J.Boschung, A. Nauels, Y. Xia, V. Bex and P.M. Midgley (eds.)]. Cambridge University Press, Cambridge, United Kingdom and New York, NY, USA, 1535 pp., (2013)

Krol, M., Houweling, S., Bregman, B., van den Broek, M., Segers, A., van Velthoven, P., …Bergamaschi, P., The two-way nested global chemistry-transport zoom model TM5 : algorithm and applications, Atmos.Chem.Phys., 5, 417-432 (2005)

Lan, X., Tans, P., Sweeney, C., Andrews, A., Dlugokencky, E., Schwietzke, S., et al. (2019). Long-term measurements show little evidence for large increases in total U.S. methane emissions over the past decade. *Geophysical Research Letters*, *46*, 4991–4999. https://doi.org/10.1029/ 2018GL081731.

Lavaux, T., Giron, C., Mazzolini, M., D'Aspremont, A., Duren, R., Cusworth, D., Shindell, D., & Ciais, P. (2022). Global assessment of oil and gas methane ultra-emitters. *Science*, *375*(6580), 557–561. https://doi.org/10.1126/science.abj4351.

Lorente, A., Borsdorff, T., Butz, A., Hasekamp, O., aan de Brugh, J., Schneider, A., Wu, L., Hase, F., Kivi, R., Wunch, D., Pollard, D. F., Shiomi, K., Deutscher, N. M., Velazco, V. A., Roehl, C. M., Wennberg, P. O., Warneke, T., and Landgraf, J.: Methane retrieved from TROPOMI: improvement of the data product and validation of the first 2 years of measurements, Atmos. Meas. Tech., 14, 665–684, https://doi.org/10.5194/amt-14-665-2021, 2021.

Lunt, M. F., Palmer, P. I., Feng, L., Taylor, C. M., Boesch, H., and Parker, R. J.: An increase in methane emissions from tropical Africa between 2010 and 2016 inferred from satellite data, Atmos. Chem. Phys., 19, 14721–14740, https://doi.org/10.5194/acp-19-14721-2019, 2019.

Membrive O. 2016, Caractérisation de la distribution verticale des gaz à effet de serre CO2 et CH4 par mesures sous ballons. Application à la validation d'observations satellites. Université Pierre et Marie Curie - Paris VI, France (https://tel.archives-ouvertes.fr/tel-01525863/document)

MethanePledge, https://www.globalmethanepledge.org/

Nisbet et al., Methane mitigation : methods to reduce emissions, on the path to the Paris agreement, Reviews of Geophysics, doi.10.1029/2019RG000675 (2020)

NOAA, https://www.noaa.gov/news-release/increase-in-atmospheric-methane-set-another-record-during-2021 (2022)

Pandey, Gautam, Houweling, Denier vd Gon, Sadavarte, Borsdorff, Hasekamp, Landgraf, Tol, van kempen, Hoogeveen, van Hees, Hamburg, Maasakkers and Aben, Satellite observations reveal extreme methane leakage from a natural gas well blow out, PNAS, doi.10.1073/pnas.1908712116 (2019)

Rödenbeck, C. (2005). Estimating CO_2 sources and sinks from atmospheric mixing ratio measurements using a global inversion of atmospheric transport. Max-Planck-Institut für Biogeochemie, Technical Report 6, 1–61.

Saunders, R., Hocking, J., Turner, E., Rayer, P., Rundle, D., Brunel, P., Vidot, J., Roquet, P., Matricardi, M., Geer, A., Bormann, N., and Lupu, C.: An update on the

RTTOV fast radiative transfer model (currently at version 12), Geosci. Model Dev., 11, 2717-2737, https://doi.org/10.5194/gmd-11-2717-2018, 2018.

Scarpelli, T. R., Jacob, D. J., Grossman, S., Lu, X., Qu, Z., Sulprizio, M. P., Zhang, Y., Reuland, F., Gordon, D., and Worden, J. R.: Updated Global Fuel Exploitation Inventory (GFEI) for methane emissions from the oil, gas, and coal sectors: evaluation with inversions of atmospheric methane observations, Atmos. Chem. Phys., 22, 3235–3249, https://doi.org/10.5194/acp-22-3235-2022, 2022.

Schneising, O., Buchwitz, M., Reuter, M., Bovensmann, H., Burrows, J. P., Borsdorff, T., Deutscher, N. M., Feist, D. G., Griffith, D. W. T., Hase, F., Hermans, C., Iraci, L. T., Kivi, R., Landgraf, J., Morino, I., Notholt, J., Petri, C., Pollard, D. F., Roche, S., Shiomi, K., Strong, K., Sussmann, R., Velazco, V. A., Warneke, T., and Wunch, D.: A scientific algorithm to simultaneously retrieve carbon monoxide and methane from TROPOMI onboard Sentinel-5 Precursor, Atmos. Meas. Tech., 12, 6771-6802, https://doi.org/10.5194/amt-12-6771-2019, https://doi.org/10.5194/amt-12-6771-2019, 2019.

Schneising, O., Buchwitz, M., Reuter, M., Vanselow, S., Bovensmann, H., and Burrows, J. P.: Remote sensing of methane leakage from natural gas and petroleum systems revisited, Atmos. Chem. Phys., 20, 9169-9182, https://doi.org/10.5194/acp-20-9169-2020, 2020.

Schuit et al., Automated detection and monitoring of methane super-emitters using satellite data, Atmos.Chem.Phys.Disc., doi:org/10.5194/acp-2022-862 (2023)

Siddans, R., Knappett, D., Kerridge, B., Waterfall, A., Hurley, J., Latter, B., Boesch, H., and Parker, R.: Global height-resolved methane retrievals from the Infrared Atmospheric Sounding Interferometer (IASI) on MetOp, Atmos. Meas. Tech., 10, 4135–4164, https://doi.org/10.5194/amt-10-4135-2017, 2017.

Siddans, R.; Walker, J.; Latter, B.; Kerridge, B.; Gerber, D.; Knappett, D.: RAL Infrared Microwave Sounder (IMS) temperature, water vapour, ozone and surface spectral emissivity. Centre for Environmental Data Analysis, doi:10.5285/489e9b2a0abd43a491d5afdd0d97c1a4, 28 June 2018.

Siddans, R.; Knappett, D.; Kerridge, B.; Latter, B.; Waterfall, A.: STFC RAL methane retrievals from IASI on board MetOp-A, version 2.0. Centre for Environmental Data Analysis, 10 March 2020. doi:10.5285/f717a8ea622f495397f4e76f777349d1, 2020.

UNEP-CCAC, United Nations Environment Programme and Climate and Clean Air Coalition, Global Methane Assessment : Benefits and costs of mitigating methane emissions, Nairobi, (2021)

Wofsy, S.C., and ATom Science Team. ATom: Aircraft Flight Track and Navigational Data. ORNL DAAC, Oak Ridge, Tennessee, USA. https://doi.org/10.3334/ORNLDAAC/1613, 2018.

Worden, *J. R., Bloom, A. A., Pandey, S., Jiang, Z., Worden, H. M., Walker, T. W., Houweling,*
S. and Röckmann, T.: Reduced biomass burning emissions reconcile conflicting estimates of the post-2006 atmospheric methane budget, Nat Commun, 1–11, doi:10.1038/s41467-017-02246-0, (2017)

Zhang, Y., Jacob, D. J., Lu, X., Maasakkers, J. D., Scarpelli, T. R., Sheng, J.-X., Shen, L., Qu, Z., Sulprizio, M. P., Chang, J., Bloom, A. A., Ma, S., Worden, J., Parker, R. J., and Boesch, H.: Attribution of the accelerating increase in atmospheric methane during 2010–2018 by inverse analysis of GOSAT observations, Atmos. Chem. Phys., 21, 3643–3666, https://doi.org/10.5194/acp-21-3643-2021, 2021.

Annex : Promotion and Scientific Publication (D11/D12/D13)

List of conference contributions :

- Aben et al., Methane+, IWGGMS-17, 14-17 June 2021
- Aben et al., Methane+ : combining SWIR and TIR measurements from space to disentangle sources and sinks of CH4, ESA Living Planet Conference, 23-27 May 2022
- Buchwitz, M., Schneising, O., Noel, S., Reuter, M., Vanselow, S., Bovensmann, H., and Burrows, J. P., Sentinel-5 Precursor methane and carbon monoxide column retrievals and assessments related to localized emission sources,EGU General Assembly 2020, 4–8 May 2020, https://doi.org/10.5194/egusphere-egu2020-7861
- Buchwitz, M., Schneising, O., Vanselow, S., Reuter, M., Bovensmann, H., Burrows, J. P., Aben, I., Landgraf, J., Lorente, A., Borsdorff, T., Retscher, C., Comparison of operational and scientific Sentinel-5-Precursor XCH4 retrievals over methane emission hotpot areas, IWGGMS-17, 14-17 June 2021, https://cce-datasharing.gsfc.nasa.gov/files/conference_presentations/Poster_Buchwitz__8_25.pdf
- Houweling et al., Constraining global methane emissions using TROPOMI data, IWGGMS-17, 14-17 June 2021
- Houweling, Recent changes in global CH4 emissions constrained by TROPOMI and IASI data, ESA ATMOS conference, 22-26 Nov. 2021
- Houweling et al., Recent changes in global CH4 emissions constrained by TROPOMI and IASI data, ESA Living Planet, 23-27 May 2022
- Lorente et al., TROPOMI XCH4 full-physics retrieval : Ocean sunglint obseravtions and surface reflecxtance spectral features, ESA Living Planet, 23-27 May 2022
- Schneising, O., Buchwitz, M.,Reuter, M., Vanselow, S., Bovensmann, H., Burrows, J. P.
  Quantification of local methane emissions from the energy sector, IWGGMS-17, 14-17 June 2021, https://cce-datasharing.gsfc.nasa.gov/files/conference_presentations/Poster_Schneising__75_25.pdf
- Schneising, O., Buchwitz, M.,Reuter, M., Vanselow, S., Bovensmann, H., Burrows, J. P. Quantification of Local Anthropogenic Methane Emissions using TROPOMI onboard Sentinel-5P, ESA ATMOS conference, 22-26 Nov. 2021, https://atmos2021.esa.int/iframe-agenda/files/Contribution_158_final_extabs.pdf
- Van Peet, Houweling, S., Marshall, J., Ramirez, T.N., Segers, A., Inverse modelling of global methane emissions using TROPOMI, EGU 2021

Most of the presentations/posters can be found on the project ftp in the folder CONFERENCES, some are also available in the public domain.

List of scientific peer reviewed papers with contributions from Methane+ :

- Lorente, A., Borsdorff, T., Butz, A., Hasekamp, O., aan de Brugh, J., Schneider, A., Wu, L., Hase, F., Kivi, R., Wunch, D., Pollard, D. F., Shiomi, K., Deutscher, N. M., Velazco, V. A., Roehl, C. M., Wennberg, P. O., Warneke, T., and Landgraf, J.: Methane retrieved from TROPOMI: improvement of the data product and validation of the first 2 years of measurements, Atmos. Meas. Tech., 14, 665–684, https://doi.org/10.5194/amt-14-665-2021, 2021.
- Lorente, A., Borsdorff, T., Martinez-Velarte, M., Butz, A., Hasekamp, O.P., Wu,L., and Landgraf, J., Evaluation of the methane full-physics retrieval applied to TROPOMI ocean sun glint measurements, Atmos. Meas. Tech., 15, 6585-6603 https://doi.org/10.5194/amt-2022-197 (2022)
- Schneising, O., Buchwitz, M., Reuter, M., Vanselow, S., Bovensmann, H., and Burrows, J. P.: Remote sensing of methane leakage from natural gas and petroleum systems revisited, Atmos. Chem. Phys., 20, 9169–9182, https://doi.org/10.5194/acp-20-9169-2020, 2020.